THE ASTROPHYSICAL JOURNAL, Vol. 159, February 1970

THE UNUSUAL COMPOSITION OF +39°4926*

KEIICHI KODAIRA,† JESSE L. GREENSTEIN, AND J. B. OKE
Mount Wilson and Palomar Observatories, Carnegie Institution of Washington,
California Institute of Technology
Received 1969 June 13

ABSTRACT

The extremely metal-poor star, +39°4926 has T_e + 7500° K, log g = 1, and a very large Balmer jump (1.7 mag). Model atmospheres explain the hydrogen spectrum, and over plausible ranges of T_e the abundances are insensitive to errors in T_e. Weak lines of He I are present, but the He/H ratio is temperature-dependent. Strong lines of C I and O I are observed and yield abundance ratios C/H and O/H near that in the Sun and insensitive to T_e. The metal abundances average 1 percent of their solar values, differ from element to element, and show an excessively large odd-even alternation.

The velocity seems variable in a long period. The absolute magnitude is near −3, the mass less than the Sun. The unusual location of the star in the H-R diagrams for either Population I or Population II may be connected with rapid evolution with mass exchange.

Nucleosynthesis of C and O may have occurred rapidly in exploding stars early in the history of the Galaxy. C, O, and products of helium burning were rapidly synthesized. Alternatively, the star may have synthesized C and O rapidly in its interior, at a time when it was more massive. The odd-even alternation suggests that α-particle capture has been particularly important; neutron-capture products are rare.

I. INTRODUCTION

The ninth-magnitude star +39°4926 is an unusual late A or early F star of low surface gravity, far from the galactic plane (l^{II} = 98°, b^{II} = −16°). Its spectrum was noted as interesting by Greenstein in 1961; a series of early spectra showed sharp Balmer lines visible up to n = 27, and extremely weak metallic lines. Several conspicuous lines, however, proved to be C I and O I. Oke's scans showed that the star had the largest observed Balmer jump (BJ = 1.7 mag). Oke, Greenstein, and Gunn (1966) derived rough parameters for the atmosphere ($\theta_e \approx 0.77$, log $g \approx 1$ from the scanner data, and $\theta_e \approx 0.68$ from the Hγ profile); they concluded that the star might be related to the W Virginis stars. In this paper, we examine the entire observational material in detail. We find $\theta_e = 0.67$ and log g = 1.20; helium seems to be 10 times more abundant than normal, which makes log g = 0.95. The abundances of the other light elements are nearly the same as those in the Sun, while the metals show as extreme a deficiency as that found in the high-velocity Population II stars; the ratio of heavier elements to light elements is even lower.

The spectrograms analyzed are listed in Table 1. The radial velocities given were measured on all plates, but the line intensities were measured with the Caltech linear microphotometer only on those so indicated in Table 1. Identifications and equivalent widths are tabulated in Table 2; when the blending by Balmer-line wings should be considered, the depth of the wings is tabulated. Colons indicate uncertain W_λ; question marks, doubtful identifications; plus signs, the presence of an unknown contributor. *Revised Multiplet Table* (RMT) numbers are also given. Some lines of He I, N I, Ne I, S I are highly uncertain but are included because of the importance of abundances of these elements. Numerous C I lines of special interest are shown in Table 3. Their identifications are referred to the work by Johansson (1966) with j-values from his work reflecting the complex-coupling scheme. Even more extensive stellar identifications of C I in the

* This research was supported in part by the U.S. Air Force under grant AFOSR 68-1401, monitored by the Air Force Office of Scientific Research of the Office of Aerospace Research.

† On leave from Tokyo Observatory, University of Tokyo.

carbon-rich star R CrB are given by Keenan and Greenstein (1963). The Na I D-lines and the H- and K-lines of Ca II in +39°4926 are blended with either interstellar or circumstellar components, which are discussed below.

The measured W_λ were compared and found to agree systematically from plate to plate, except between two 27 Å mm^{-1} Pd plates taken on 103aF, namely, 8831 and 8836. The equivalent widths in the yellow and red are of only moderate quality; weak lines in the blue, at 9 Å mm^{-1}, scatter by up to ± 0.3 in log W_λ. Individual pairs of plates give more typically ± 0.2 as the difference in log W_λ, so that log W_λ based on four plates should be good to ± 0.07. The Balmer-line profiles Hβ, Hγ, and Hδ were measured at 9 Å mm^{-1}, and Hα and Hβ were available at 27 Å mm^{-1}. Tables 4A and 4B give the residual intensity r for each plate and for each wing.[1] Within the accuracy of measurement the plates agree within $\Delta r \leq 0.04$; Hβ, however, visible at both 9 and 27 Å mm^{-1}, shows a systematic difference. This may be caused by its location at opposite ends of the sensitivity range of the two emulsions. For this reason, also, the W_λ are most uncertain

TABLE 1

COUDÉ SPECTRA AND VELOCITIES OF +39°4926

Plate	Date	Emulsion	W_λ	Velocity (km sec^{-1})	Dispersion (Å mm^{-1})
Pd 6268	1961 Nov. 14	IIaO Bkd.	...	-16.8 ± 4.0	18
Pd 7433	1963 Aug. 1	IIaO Bkd.	...	-31.3 ± 4.0	18
Pd 7542	1963 Sept. 9	IIaF	X	-28.7 ± 6.0	27
Pc 8251	1964 Sept. 26	IIaO Bkd.	X	-28.3 ± 2.0	9
Pc 8333	1964 Nov. 22	IIaO Bkd.	X	-30.8 ± 2.0	9
Pc 8822	1965 Aug. 5	IIaO Bkd.	X	-44.6 ± 2.0	9
Pc 8826	1965 Aug. 6	IIaO Bkd.	X	-43.2 ± 2.0	9
Pd 8831	1965 Aug. 8	103aF	X	-43.0 ± 6.0	27
Pd 8836	1965 Aug. 9	103aF	X	-47.4 ± 6.0	27
Pc 8837	1965 Aug. 9	IIaO Bkd.	...	-44.4 ± 2.0	9
Pc 8967	1965 Oct. 4	IIaO Bkd.	X	-26.9 ± 2.0	9
Pd 8972	1965 Oct. 5	IIaF	X	-33.2 ± 6.0	27
Pc 10233	1967 Aug. 18	IIaO Bkd.	...	-44.7 ± 2.0	9

in the $\lambda\lambda$4900–5000 region; similarly, W_λ is poor at $\lambda < 3800$ Å and $\lambda > 6700$ Å. The mean hydrogen-line profiles in Figure 9 are obtained by averaging violet and red wings. The highest visible member of the Balmer series was $n = 27$, observed on Pc 10233 and Pd 6268. The spectra are thinly exposed in the ultraviolet, and the separation of successive Balmer lines is $\Delta\lambda = 1.5$ Å, comparable with the observed widths of weak metallic lines ($\Delta\lambda = 0.5$ Å on Pc and 1 Å on Pd). Therefore, $n = 27$ is a lower limit to the true "last member" of the Balmer series.

II. SCANS

Both the Mount Wilson and Palomar photoelectric spectrum scanners were used, and Table 5 shows the measured values, on different dates, of $m = -2.5 \log f_\nu +$ constant, on the scale of Oke (1964, 1965). The unit of f_ν is ergs sec^{-1} cm^{-2} (Hz)$^{-1}$. The "mean" column gives an unweighted mean, since the consistency of data taken on different nights is excellent. The errors Δm are ± 0.03 in the blue and ± 0.05 in the ultraviolet and red; larger errors exist only in the infrared at the limit of the cathode sensitivity. The standard normalization of the magnitude scales by Oke (1964, 1965) is based on the nonblanketed model of Vega by Mihalas (1965) with $\theta_e = 0.53$ and $\log g = 4.44$. Recent discussions with new, blanketed models assume lower gravity for Vega (see Strom,

[1] Three significant figures are given only for convenience in smooth plotting.

TABLE 2

IDENTIFICATIONS AND EQUIVALENT WIDTHS

λ(Å)	W_λ(mÅ)	Identification	Remarks
3748.49		FeII(154)	H_{12} bl
50.15		H_{12}	
58.24	39::	FeI(21)	
59.29	47	TiII(13)	
61.32	82::	TiII(13)	
70.63		H_{11}	
83.35	52::	FeII(14)	
97.90		H_{10}	
3819.40	41::	HeI(22)	
20.43	40:	FeI(20)	
24.91		FeII(29)	
25.88	49:	FeI(20)	
29.35	73	MgI(3)	17% H_9
32.30	81	MgI(3),MgI(3)	50% H_9
35.39		H_9	
38.29	117:	MgI(3)	37% H_9
53.66	26:	SiII(1)	
56.02	70	SiII(1)	
57.35	15::		
59.91	24	FeI(4)	
62.59	40	SiII(1)	
89.05		H_8	
3900.55	37	TiII(34)	
13.46	42	TiII(34)	
33.66	507	CaII K	
35.95	25::	FeII(137)+	
42.22	15::	CI	
44.01	4::	AℓI(1)	
47.5	68	OI(3),OI(3),OI(3)	
51.8	18:		
54.69	22	OI(30)+	
61.52	15:	AℓI(1)	8%
68.47		CaII H	
70.07		Hε	
4009.2	18		
09.93	10::	CI	
21.6	10::		
26.2	21:	HeI(18),HeI(18)	
29.41	12::	CI	
45.82	25	FeI(43)	
63.60	16	FeI(43)CI(7)	Partially
64.27	14::	CI(7)?	blended
65.25	16::	CI(7)?	
67.2	14::		
71.74	18	FeI(43)	
72.64	7::	CI	
77.71	11	SrII(1)	
4101.74		Hδ	
09.9	30::	NI(10)+?	
28.05	25	SiII(3)	
30.88	32	SiII(3)	
36.5	12:	FeI(694)+?	
46.9	12		
51.46	6::	NI(6)?	
71.90	8::	TiII(105)?	
73.45	28	FeII(27)	
77.87	9:	YII(14)	
78.86	35	FeII(28)	
90.74	12:	SiII	
4202.03	10::	FeI(42)	
15.52	9::	SrII(1)	
23.17	21	CI,CI,CI	

λ(Å)	W_λ(mÅ)	Identification	Remarks
4228.33	28	CI(17)	
33.17	108	FeII(27)	
35.94	16::	FeI(152)	
42.1	18		
46.83	23	ScII(7)	
58.16	15::	FeII(28)	
4269.02	28	CI(16)	
71.76	23	FeI(42)	
90.22	18	TiII(41)	
94.11	14:	TiII(20),FeI(41)	
96.57	18	FeII(28)	
4300.05	24	TiII(41)	
03.17	35	FeII(27)	
05.0	11::		
07.90	12:	TiII(41),FeI(42)	
14.1	22	ScII(15),FeII(32)	
20.75	18:	ScII(15)	
23.85	20::		
25.01	11:	ScII(15)	2% Hγ
25.76	23	FeI(42)	3% Hγ
40.47		Hγ	
51.8	88	FeII(27),MgI(14), MgI(14)	
68.30	58	OI(5)	
71.37	36	CI(14)	
74.45	15	ScII(14),YII(13)	
79.24	16::		
81.1	14::	CrI(64)+?	
83.55	25	FeI(41)	
85.38	18:	FeII(27)	
95.03	30	TiII(19)	
4404.75	17:	FeI(41)	
08.4	12::	FeI(68)+	
15.43	13	FeI(41),ScII(14)	
16.82	21	FeII(27)	
17.72	15:	TiII(40)	
36.6	18:		
43.80	20	TiII(19)	
66.48	11	CI	
68.49	12	TiII(31)	
71.47	23::	HeI(14)?	
4477.47	9::	CI	
78.6	25:	CI,CI,CI	
81.29	179	MgII(4),MgII(4)	
89.19	16	FeII(37)	
91.40	9::	FeII(37)	
4501.27	15	TiII(31)	
08.28	45	FeII(38)	
15.34	27	FeII(37)	
20.23	25	FeII(37)	
22.63	48	FeII(38)	
33.97	34	TiII(50)	
41.52	28	FeII(38)	
49.5	108	FeII(38),TiII(82)	
52.0	36::		
55.89	34	FeII(37)	
58.66	26	CrII(44)	
63.76	24:	TiII(50)	
71.97	18	TiII(82)	
74.5	15::	CrI(148)+?	
83.83	78	FeII(38)	
88.22	18	CrII(44)	
4618.83	19	CrII(44)	
29.34	37	FeII(37)	
34.11	15:	CrII(44)	

TABLE 2 (CONT'D)

λ(Å)	W_λ(mÅ)	Identification	Remarks
4679.0	21::		
94.3	11::	SI(2)?	
95.8	10::	SI(2)?	
96.6	4::	SI(2)?	
98.9	27::		
4734.26	16::	CI	
38.47	28::	CI,CI+MnII(5)?	
62.4	69	CI(6),CI(6)	
66.68	24	CI(6)	
70.03	24	CI(6)	
4771.75	60	CI(6)	
73.5	19	OI(16),OI(16), OI(16)	
75.91	40	CI(6)	
4824.13	22::	CrII(30)	
48.24	20:	CrII(30)	5% Hβ
61.33	Hβ		
76.41	18::	CrII(30)	4% Hβ
96.4	32:		
99.47	47::		
4923.92	108	FeII(42)	
32.00	69:	CI(13)	
57.2	39::	FeI(318), BaII(10)+?	
68.76	28::	OI(14),OI(14), OI(14)	
5018.43	147	FeII(42)	
41.06	36::	SiII(5)	
52.12	98	CI(12)	
56.5	56::	SiII(5),SiII(5)	
5121.0	46:		
69.03	135	FeII(42)	
72.68	124	MgI(2)	
83.60	150	MgI(2)	
5255.0	52:		
5329.5	148	OI(12),OI(12), OI(12)	
80.35	67	CI	
5401.0	40	NeI(3)+	
36.5	97	OI(11),OI(11), OI(11)	
81.2	35:		
5513.7	45:		
18.7	21:		
26.2	32:		
88.8	35:		
94.8	27:		
5600.2	37		
5696.4	59:		
98.8	20:		
5705.8	50	SI(11)?	
18.4	33:		
81.4	135		
5838.0	32		
44.3	50:		
89.9	860	NaD_2,ISD_2	
95.9	670	NaD_1,ISD_1	
5959.0	98	OI(23),OI(23), OI(23)	atm. ℓ. blended
78.0	52	SiII(4)	atm. ℓ. blended
6001.13	43	CI	
06.0	30	CI	Partially blended
07.2	45	CI	
10.7	54	CI	
13.5	124	CI,CI,CI	
46.4	38	OI(22),OI(22), OI(22)+SI(10)?	
52.7	30::	SI(10)?	
6149.2	38	FeII(74)+	
56.8	264	OI(10),OI(10), OI(10)	
6203.5	30:		
6347.09	74	SiII(2)	
71.36	35	SiII(2)	
6402.3	8::	NeI(1)?	
55.5	60	OI(9),OI(9), OI(9),FeII(74)	
69.8	25:		
6562.82		Hα	
87.23	92	CI	+ atm. ℓ. 5% Hα
6645.0	25::	NI(20)?	
53.4	32		
57.0	60::		
6743.5	44::	SI(8)?	
48.6	43::	SI(8)?	
57.1	71::	SI(8)?	
67.3	35:		
69.3	49::		
76.2	48::		
91.7	42:		

TABLE 3

C I LINES OBSERVED IN +39°4926

Term Lower	Term Upper	J_ℓ	J_u	λ(Å)	RMT	W_λ	Remarks
$3s\,^1P^o$	$4p\,^1S$	1	0	4932.050	(13)	69	
	^1P	1	1	5380.336	(11)	67	
	^1D	1	2	5052.167	(12)	98	
$3s\,^1P^o$	$5p\,^1S$	1	0	4228.326	(17)	28	
	^1P	1	1	4371.368	(14)	36	
	^1D	1	2	4269.020	(16)	28	
$3s\,^1P^o$	$6p\,^1S$	1	0	3942.223		15::	
	^1P	1	1	4009.930		10::	
$3s\,^3P^o$	$4p\,^3P$	1	0	4770.032	(6)	24	
		2	2	4771.747	(6)	60	
		2	1	4775.907	(6)	40	
		1	1	4766.676	(6)	24	
		0	1	4762.314	(6)	69	
			2	4762.541	(6)		
$3s\,^3P^o$	$5p\,^3P$	2	2	4029.413		12::	
	^3D	1	2	4064.271	(7)	14::	
		0	1	4063.577	(7)	16	blend with Fe I
		2	3	4065.246	(7)	16::	
$3p\,^1P$	$4d\,^1P^o$	1	1	6587.608	(22)	92	5% Hα + atm. ℓ.
$3p\,^3D$	$5d\,^3D$	3	2	6006.028		30	
	^3F	3	4	6013.215		124	blend with λ6014
$3p\,^3D$	$6s\,^3P^o$	3	2	6013.215			
		1	1	6007.178		45	
		1	0	6010.679		54	
		2	2	6001.126		43	
		2	1	6014.845		124	blend with λ6013
$2p'\,^3D^o$	$5p\,^3P$	1	1	4738.213		28::	blend with MnII?
		2	1	4738.466			
		3	2	4734.262		16::	
$2p'\,^3D^o$	5fF	3	$(3\frac{1}{2})_{3,4}$	4477.472		9::	
		2	$(3\frac{1}{2})_{3}$	4478.319			
		1	$(2\frac{1}{2})_{2}$	4478.588		25::	
		2	$(2\frac{1}{2})_{2,3}$	4478.825			
	G	3	$(3\frac{1}{2})_{3,4}$	4466.677		11	
$2p'\,^3D^o$	6fF	2	$(2\frac{1}{2})_{2,3}$	4223.360			
		2	$(3\frac{1}{2})_{3}$	4223.159		21	
		1	$(2\frac{1}{2})_{2}$	4223.159			
$2p'\,^3D^o$	7fG	3	$(3\frac{1}{2})_{3,4}$	4072.643		7::	

TABLE 4A

RESIDUAL INTENSITY IN THE BALMER LINES

MEASURED ON IIaO PLATES

	Δλ (Å)	Pc 8251		Pc 8822		Pc 8826		Pc 8967	
		red	violet	red	violet	red	violet	red	violet
	0	0.082	0.082	0.109	0.109	0.026	0.026	0.041	0.041
	1	.345	.339	.381	.374	.369	.362	.374	.326
	2	.467	.485	.502	.503	.523	.495	.519	.485
	4	.682	.698	.700	.712	.726	.708	.722	.691
Hδ	6	.817	.824	.834	.831	.852	.834	.825	.813
	8	.903	.900	.904	.911	.930	.937	.878	.891
	10	.943	.940	.949	.951	.968	.973	.924	.921
	15	0.984	0.987	.985	.979	0.992	-----	.969	.963
	20	-----	-----	0.985	0.990	-----	-----	0.969	.978
	0	0.104	0.104	0.117	0.117	0.092	0.092		
	1	.375	.341	.403	.391	.382	.389		
	2	.479	.480	.530	.513	.493	.500		
	4	.657	.689	.705	.709	.689	.692	disturbed	
Hγ	6	.800	.819	.818	.823	.825	.817		
	8	.874	.887	.899	.900	.901	.897		
	10	.923	.940	.933	.950	.954	.937		
	15	.985	-----	.978	.985	0.966	0.989		
	20	1.000	-----	0.989	0.989	-----	-----		
	0	0.074	0.074	0.025	0.025	0.061	0.061	0.176	0.176
	1	.394	.405	.457	.422	.414	.453	.433	.423
	2	.538	.530	.554	.545	.535	.571	.522	.536
	4	.705	.690	.710	.706	.697	.694	.662	.660
Hβ	6	.820	.801	.817	.825	.811	.790	.775	.771
	8	.886	.890	.890	.890	.900	.882	.858	.853
	10	.928	.933	.901	.930	0.947	0.949	.910	.899
	15	0.980	0.966	0.969	0.972	-----	-----	0.952	0.961

TABLE 4B

RESIDUAL INTENSITY IN THE BALMER LINES

MEASURED ON IIaF AND 103aF PLATES

	Δλ (Å)	Pd 7542		Pd 8831		Pd 8836		Pd 8972	
		red	violet	red	violet	red	violet	red	violet
	0	0.238	0.238	0.205	0.205	0.202	0.202		
	1	.571	.501	.475	.411	.388	.357		
	2	.657	.613	.566	.525	.571	.569		
	4	.783	.755	.691	.687	.729	.709	not observed	
Hβ	6	.852	.850	.789	.806	.829	.808		
	8	.904	.900	.858	.878	.890	.888		
	10	.940	.941	.902	.945	.940	.931		
	15	0.983	0.991	0.972	0.992	0.978	0.969		
	0	0.283	0.283	0.344	0.344	0.294	0.294	0.322	0.322
	1	.637	.612	.573	.568	.584	.614	.573	.615
	2	.696	.693	.676	.687	.698	.692	.674	.670
	4	.762	.769	.754	.753	.778	.761	.777	.739
	6	.806	.816	.815	.808	.828	.821	.826	.802
Hα	8	.845	.849	.850	.847	.865	.862	.860	.844
	10	.869	.883	.879	.876	.893	.890	.881	.871
	15	.914	.930	.931	.921	.949	.938	.924	.920
	20	.936	.956	.952	.958	.968	.964	.941	.943
	25	.946	.968	.961	.973	.972	.976	.963	.951
	30	0.948	0.973	0.969	0.980	0.975	0.985	0.969	0.954

TABLE 5

SCANNER RESULTS

OBSERVED MONOCHROMATIC MAGNITUDES

$m = 2.5 \log f_{\nu} + \text{const.}$

λ(Å)	1/λ(μ^{-1})	Sept.13 1962	Sept.23 1963	Sept.27 1963	Sept.28 1963	Sept.30 1963	Nov.30 1963	Dec.1 1963	Sept.16 1964	Oct.17 1964	Mean	Δm(Vega)
3390	2.950	----	11.07	11.17	----	----	11.10	11.17	11.23	11.20	11.16	+0.06
3448	2.900	----	11.08	11.12	----	----	11.05	11.11	11.14	11.08	11.10	+0.06
3509	2.850	----	11.07	11.09	----	----	10.99	11.07	11.10	11.04	11.06	+0.06
3571	2.800	----	11.01	11.03	----	----	10.97	11.08	11.03	11.00	11.02	+0.06
3636	2.750	----	10.95	10.97	----	----	10.93	10.98	11.00	10.94	10.96	+0.06
3704	2.700	----	10.41	10.33	----	----	10.36	10.32	10.43	10.44	10.38	+0.06
3862	2.589	9.44	9.41	9.56	----	----	-----	-----	9.24	9.41	9.41	-0.07
4032	2.480	9.31	9.31	9.28	----	----	9.27	9.33	9.27	9.23	9.28	-0.05
4167	2.400	9.32	9.30	9.29	----	----	9.27	9.33	9.28	9.29	9.30	-0.04
4255	2.350	9.31	9.29	9.29	----	----	9.27	9.33	9.27	9.27	9.29	-0.04
4464	2.240	9.29	9.27	9.26	----	----	9.24	9.26	9.25	9.25	9.26	-0.02
4566	2.190	9.28	9.25	9.26	----	----	9.24	9.27	9.24	9.23	9.25	-0.01
4785	2.090	9.27	9.23	9.26	----	----	9.33	9.28	9.25	9.23	9.26	-0.01
5000	2.000	9.22	9.21	9.26	9.25	9.26	9.18	9.26	9.23	9.22	9.23	.00
5263	1.900	9.20	9.16	9.23	9.23	9.26	9.16	9.23	9.21	9.20	9.21	.00
5556	1.800	9.18	9.10	9.18	9.21	9.18	9.15	9.21	9.20	9.19	9.18	+0.02
5882	1.700	9.14			9.21	9.25	9.13	9.14	9.18	9.16	9.17	+0.02
6055	1.652				9.17	9.23					9.20	+0.03
6370	1.570				9.18	9.22					9.20	+0.04
6800	1.471				9.16	9.22					9.19	+0.05
7100	1.408				9.14	9.24					9.19	+0.06
7530	1.328				9.18	9.23					9.20	+0.06
7850	1.274				9.17	9.21					9.19	+0.07
8080	1.238				9.19	9.27					9.23	+0.08
8400	1.190				9.10	9.22					9.16	-0.04
8805	1.136				9.08	9.10					9.09	-0.04
9700	1.031				9.05	9.10					9.07	-0.04
9950	1.005				9.00	9.09					9.04	-0.05
10250	0.976				9.09	9.12					9.10	-0.05
10400	0.962				8.98	9.13					9.05	-0.05
10800	0.926				9.00	9.15					9.07	-0.06

Gingerich, and Strom 1966; Hayes 1967; Heintze 1968; Gehlich 1969). The profiles of Balmer lines and f_ν of the Vega model are insensitive to the parameters in this range. We give in the last column the corrections Δm(Vega) from the system by Oke (1964) to a system based on the Mihalas (1966) blanketed model with $\theta_e = 0.525$, $\log g = 4.0$. This set of parameters was also suggested by both Baschek and Oke (1965) and Hardorp and Scholz (1968). The Δm(Vega) will be taken into consideration when we compare the final model of $+39°4926$ with the observations. After these corrections, a graphical derivation of the Balmer jump gives BJ $= 1.73 \pm 0.04$ mag, and the Paschen jump gives PJ $= 0.23 \pm 0.07$ mag.

III. RADIAL VELOCITY

The spectra taken at 9 Å mm^{-1} showed about twenty-five accurately measurable lines in the blue, and about ten or fewer in the visual (27 Å mm^{-1}), including the Balmer lines. The resulting radial velocities with probable errors, shown in Table 1, vary from -16.8 to -47.4 km sec^{-1}. Plotted as a function of time in Figure 1, they show a variation which possibly might be a short-period variation around a long-term trend. But a more reasonable assumption is the simple periodic variation shown in Figure 1, with a

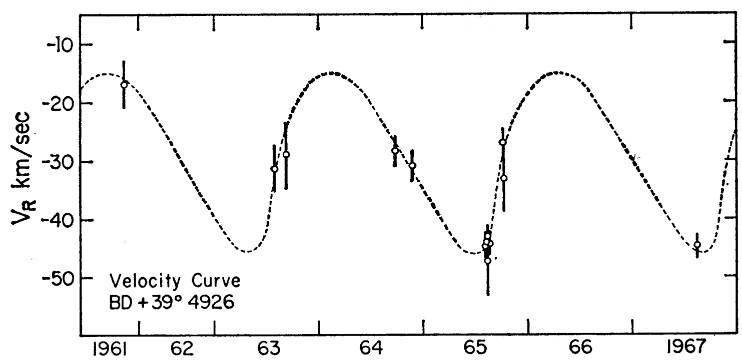

FIG. 1.—Radial velocities, with probable errors; long-term cycle fitted by dashed curve has a 775-day period.

period of 775 ± 5 days. Short periods seem to be excluded by the constancy on five plates taken from August 5 to August 9. Intrinsic pulsation with such a long period seems unlikely from the $P\rho^{1/2}$ law, and also because the fluxes and absorption-line strengths do not vary (see Tables 4A and 5). Oke, Greenstein, and Gunn (1966) suspected a small variation in $\log f_\nu$, based on the first data; this variation does not seem to be real. The variation in velocity is most probably that in a binary system. Note that the peculiar B star of Population II in Messier 13 (Stoeckly and Greenstein 1968) is also suspected of a variation in velocity. Perhaps the rare evolutionary stage of both these stars is connected with binary-star interactions.

IV. INTERSTELLAR LINES

It was noted that the Na I D-lines remained stationary at -20.5 ± 4.0 km sec^{-1} through all phases, while the Ca II H- and K-lines varied in phase with other lines. The major part of the D-lines are interstellar or circumstellar, while the K-lines are stellar. For the abundance analysis we attempted to separate the components by using the velocity variation. Figures 2 and 3 show the observed profiles and the expected position of the line centers for each component. Only a slight asymmetry for the D-lines is seen on Pd 8831 and Pd 8836, which have the largest difference between the stellar and interstellar velocities ($\Delta v_r \approx 25$ km sec^{-1}). Almost the entire strength[2] of Na I is to be assigned

[2] Weak lines of atmospheric water vapor blend with D_1 and D_2, but have negligible effect. The asymmetry common to the shortward wings of both D_1 and D_2 is used to estimate roughly the stellar contribution.

to the interstellar component, and we estimate the stellar W_λ to be 15 and 30 mÅ, respectively, for D_1 and D_2. The K-line, at higher dispersion, undergoes the more conspicuous variation shown in Figure 3. On Pc 8822 and Pc 8826, $\Delta v_r \approx 23$ km sec^{-1}, and the asymmetry is clear; on Pc 8251 and Pc 8967, where Δv_r is small, the asymmetry disappears. After correcting for the simple overlapping we found the interstellar line to have $W_\lambda = 105$ mÅ, as shown at the bottom of Figure 3. The situation is more complicated in the H-line of Ca II, blended with Hϵ. We had two plates (Pc 8822 and Pc 8826) with a mean stellar velocity of -44 km sec^{-1} and two (Pc 8251 and Pc 8967)

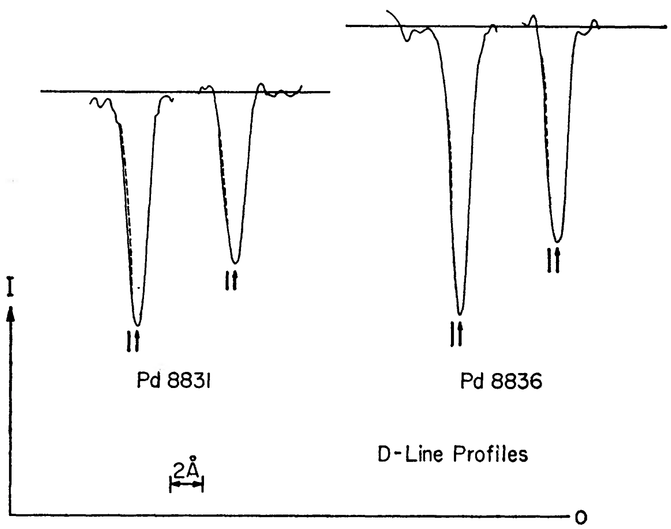

FIG. 2.—D-line profiles. *Dashed lines*, a symmetric profile obtained by reflecting the long-wavelength wing. *Arrow*, position of interstellar line; *vertical bar*, position of stellar line. Vertical scale is intensity, and wavelength increases to the right. (27 Å mm^{-1} original dispersion.)

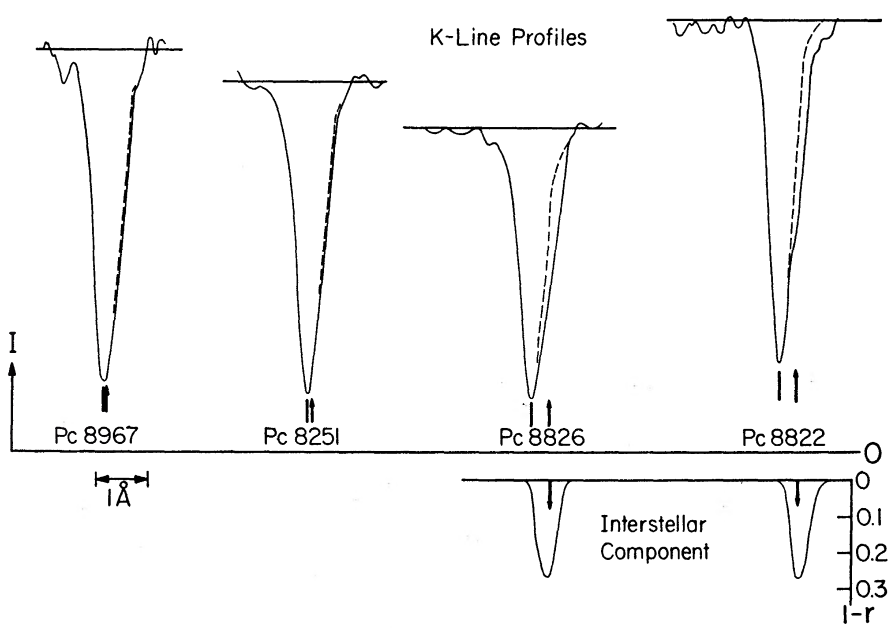

FIG. 3.—K-line profiles. *Dashed line*, reflected symmetric profile. Vertical scale is intensity. The finally deduced interstellar components, at the lower right, show the line depth, $1 - r$, uncorrected for finite resolution. *Arrow*, wavelength of interstellar component; *bar*, wavelength of stellar component.

with -27 km sec^{-1}. The mean profiles in Figure 4 show an asymmetry and shift which can be qualitatively explained as a superposition of a fixed interstellar line and a stronger stellar line of variable velocity. In Table 6 we give quantitative estimates of the strength of the stellar and interstellar lines. The strength of the stellar K-line is relatively reliable; that of the D-lines, only a very rough estimate. The interstellar Na I is much stronger than K, no matter how far we press the case for stellar D-lines. This phenomenon is commonly noted in stars of moderately high galactic latitude. The somewhat high

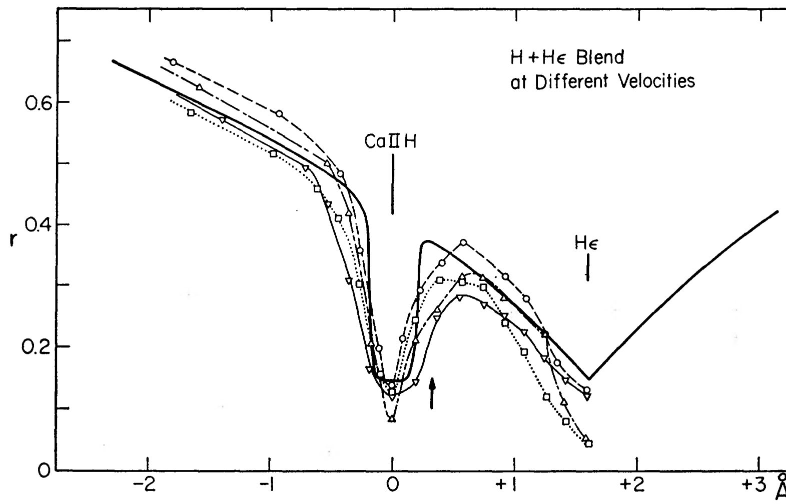

FIG. 4.—Blended profiles of Hϵ + H (stellar and interstellar). Solid line is calculated from the final model. *Arrow*, position of interstellar line. The shift and asymmetry show that the H-line is largely stellar for Pc 8833 (*open circle*) and Pc 8826 (*upright triangle*). The interstellar component nearby coincides with the stellar on Pc 8251 (*square*) and Pc 8967 (*inverted triangle*).

TABLE 6

W_λ (mÅ) OF STELLAR AND INTERSTELLAR K- AND D-LINES

Spectral Line	Total	W_λ (Stellar)	W_λ (Interstellar)
Ca II K	507	435	105
Na I:			
D_1	670	~ 15	670
D_2	860	~ 30	860

sodium-doublet ratio is reasonable for such a strong line. An argument against circumstellar origin for the D-lines is that the stationary component is at a more positive velocity than is the star. Greenstein (1968) gives interstellar D_2 line strengths up to 600 mÅ (reduced to the galactic latitude of 16°); the high-velocity CH stars show similarly strong interstellar D-lines in spite of their moderately high galactic latitude. The galactic rotation and solar motion for $l^{II} = 98°$ and a distance of 2 kpc is about -20 km sec^{-1}, as observed for the interstellar D-lines.

V. THE MODEL ATMOSPHERE

We limit the domain of parameters of the stellar atmosphere by various standard methods of estimating θ_e and g.

a) Balmer Lines

We compare the observed profiles with those given for a nonblanketed set of models by Mihalas (1965). The metallic-line blanketing is very small in +39°4926, although effects of other opacity sources such as C, C^-, and He might eventually need to be evaluated if C and He are indeed highly overabundant relative to hydrogen. We find

$$0.65 < \theta_e < 0.68 ; \quad 0.8 < \log g < 1.2 .$$

b) Balmer and Paschen Jumps

From a comparison with Mihalas (1965) the BJ = 1.73 mag and PJ = 0.23 mag lead to the same possible range as do the Balmer-line profiles.

c) Curve of Growth of Fe

From atomic data given and discussed in Table 9, curves of growth were constructed for Fe I and Fe II. A considerable number of lines existed, and the effect of atmospheric

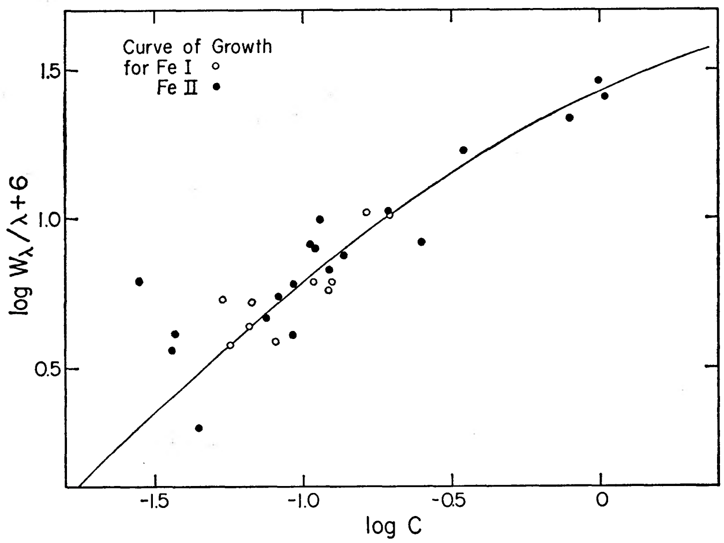

FIG. 5.—First-approximation curves of growth for Fe I (*open circles*) and Fe II (*filled circles*). Line strengths, log *C*, are defined by eq. (2). Note that the level of ionization is well defined by lines on the 45° portion for both neutral and ionized iron.

stratification should be small. The empirical curves were compared with the theoretical curve by Wrubel (1949), with $B(0)/B(1) = \frac{1}{3}$ and $\log a = -1.8$. The curves shown in Figure 5 determine a degree of excitation and ionization such that

$$\log P_e = -9.13\theta + 7.32 . \tag{1}$$

The shifts depend on the scale of laboratory *f*-values through the line-strength parameter, with the usual definition

$$\log C = \log gf\lambda - \log k_\lambda - \chi_{rs}\,\theta + \text{constant} . \tag{2}$$

The constant is zero for Fe II and -2.07 for Fe I at $\theta = 0.775$. The total Doppler parameter was found to 5.4 km sec^{-1}, or a turbulent velocity of 5.1 km sec^{-1}. The range of θ and g suggested above by the hydrogen spectrum makes this quite reasonable. For example, we derive from a model with

$$\theta_e = 0.68 , \quad \log g = 1.0$$

at $\tau_0 = 0.2$, at 5000 Å, the values close to equation (1):

$$\theta = 0.76 , \quad \log P_e = 0.30 .$$

We are then justified in calculating two approximate models M1 and M2, with atmospheric parameters shown in Table 7 and a constant microturbulent velocity of 5.1 km sec^{-1}. The opacities were taken from Bode (1965), the models from Mihalas (1965). The calculation of the radiative flux in the continuum and in the lines was made at the California Institute of Technology Computing Center; the techniques used in the calculation were essentially those developed at Kiel (see Baschek, Holweger, and Traving

TABLE 7

CHARACTERISTICS OF PRELIMINARY MODELS M1 AND M2

Model	log g	θ_e	$\Delta \log \epsilon$ Fe II/Fe I	$\Delta \log \epsilon$ Mg II/Mg I	BJ (mag)
M1....	1.0	0.65	+0.29	+0.38	1.86
M2....	1.0	0.70	−0.14	−0.32	1.55

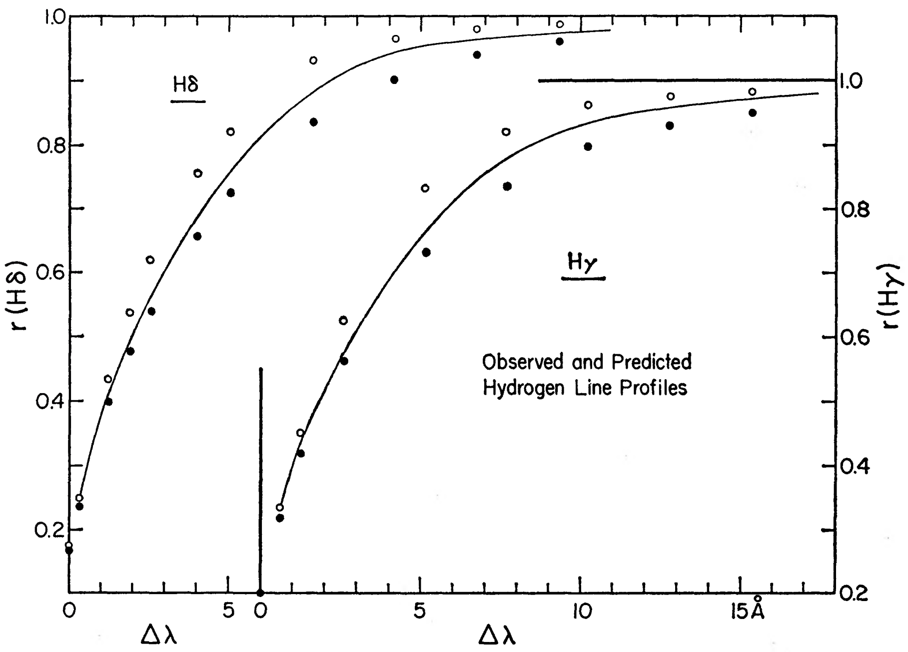

FIG. 6.—*Solid lines*, observed profiles of Hγ and Hδ; *open circles*, predictions from M1 ($\theta_e = 0.65$); *filled circles*, predictions from M2 ($\theta_e = 0.70$).

1966; Kodaira 1964). We use the level of ionization of Fe and Mg as a check. We derive abundances by number, relative to hydrogen on a scale log H = 12.00, from the observations of neutral and ionized atoms and the two models. The results given in columns (4) and (5) suggest that the true temperature lies between models M1 and M2, if log $g = 1.0$. The observed BJ, 1.73 mag, also lies between the two models. In Figure 6 we see that the observed Hγ and Hδ line profiles fall between those predicted by the two models. The line-broadening theory was that of Griem (1967). We now combine the various criteria for a best model by studying the effects of changes of θ and log P_e on observable quantities. We interpolate a network of (θ, log P_e) at $\tau_0 = 0.2$ in models in the neighborhood of M1 and M2. The observable parameters are $\Delta \log \epsilon$ for Mg and Fe, the line profiles (Hγ), and the Balmer jump (BJ). It is difficult to pinpoint (θ, g)

from Hγ and the BJ alone, because these quantities are near their maxima and vary only slowly. The ionization equilibria give a more narrowly defined best value, as is shown in Figure 7. We adopt for M3

$$\theta_e = 0.67\,, \quad \log g = 1.2\,.$$

VI. THE FINAL MODEL M3

A quadratic interpolation in the grid of models given by Mihalas (1965) was made with the above parameters and provides model M3, given in Table 8. The first output is the predicted flux from M3, which is compared with the observations in Figure 8. The effect of lines in Vega as given by Baschek and Oke (1965) is shown, and is very small. The theoretical f_ν curve for +39°4926 is not corrected for lines, but this effect must be even less than in Vega. The conspicuous and systematic deviation between theoretical and observed curves is caused by interstellar reddening, which is to be expected both

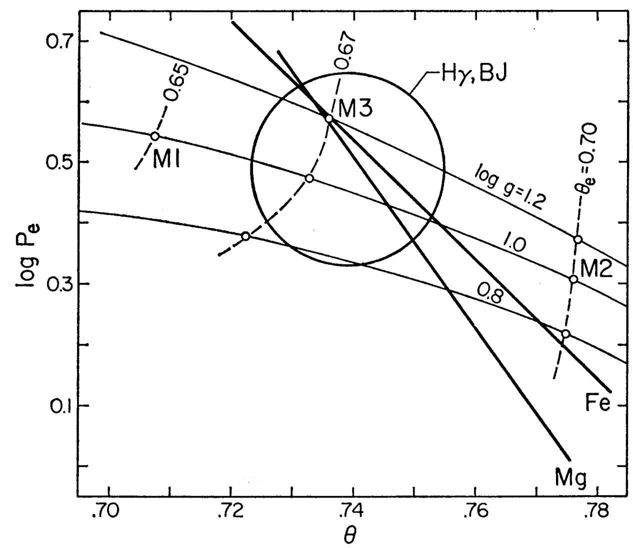

FIG. 7.—*Solid* and *dashed lines*, log P_e and θ at $\tau_0 = 0.2$ for a network of models near M1 and M2. *Circle*, domain of probable models fitting Hγ and the Balmer jump. *Heavy solid lines*, ionization equilibria from lines of Mg and Fe. The final model chosen is M3.

from the latitude and the distance of this A or F bright giant and from the strong interstellar lines. The difference between the observed and theoretical values of f_ν is converted into magnitudes, δm_ν, and plotted against λ^{-1} in inverse microns at the bottom of Figure 8. The fit with the λ^{-1} law is excellent. If the straight-line representation

$$\delta m_\nu = 0.20\,\frac{1}{\lambda} + \text{constant}\,, \qquad (3)$$

is used, the total absorption in V is 0.30 mag (Allen 1963), or a $B - V$ reddening near 0.10 mag. At $b^{\rm II} = -16°$ this is consistent with a reddening at the galactic pole of 0.03 mag. The calculated and observed hydrogen discontinuities are in good agreement.

Discontinuity	M3	Observed
BJ..........	1.71	1.73±0.04
PJ..........	0.22	0.23±0.07

1970ApJ...159..485K

TABLE 8

FINAL MODEL OF +39°4926 (M3)

$\theta_e=0.67$, log $g=1.20$, ξ (turbulent) $=5.1$ km sec^{-1}

τ	θ	T	log P_e	log P_g	$-$log κ
0.0.......	0.8577	5876	−1.486	−0.222	25.338
0.0005....	0.8569	5882	−1.416	−0.105	25.372
0.0010....	0.8561	5887	−1.338	+0.027	25.409
0.0020....	0.8549	5895	−1.160	+0.336	25.491
0.0030....	0.8528	5910	−1.043	+0.533	25.526
0.0040....	0.8511	5922	−0.956	+0.676	25.547
0.0050....	0.8496	5932	−0.889	+0.784	25.555
0.0075....	0.8461	5957	−0.760	+0.985	25.564
0.010.....	0.8432	5977	−0.668	+1.123	25.559
0.020.....	0.8325	6054	−0.437	+1.428	25.501
0.030.....	0.8239	6117	−0.293	+1.585	25.431
0.040.....	0.8158	6178	−0.183	+1.685	25.363
0.050.....	0.8083	6235	−0.096	+1.753	25.301
0.075.....	0.7917	6366	+0.079	+1.867	25.161
0.10......	0.7782	6476	+0.213	+1.933	25.040
0.20......	0.7352	6855	+0.572	+2.047	24.675
0.30......	0.7038	7161	+0.795	+2.086	24.422
0.40......	0.6784	7429	+0.955	+2.101	24.240
0.50......	0.6578	7662	+1.076	+2.107	24.097
0.75......	0.6171	8167	+1.294	+2.110	23.828
1.0.......	0.5877	8576	+1.436	+2.110	23.643
1.5.......	0.5466	9221	+1.607	+2.115	23.419
2.0.......	0.5187	9717	+1.699	+2.126	23.311
4.0.......	0.4581	11002	+1.835	+2.180	23.250
6.0.......	0.4263	11823	+1.890	+2.223	23.284
10.0.......	0.3901	12920	+1.959	+2.286	23.327
14.0.......	0.3688	13666	+2.011	+2.334	23.343

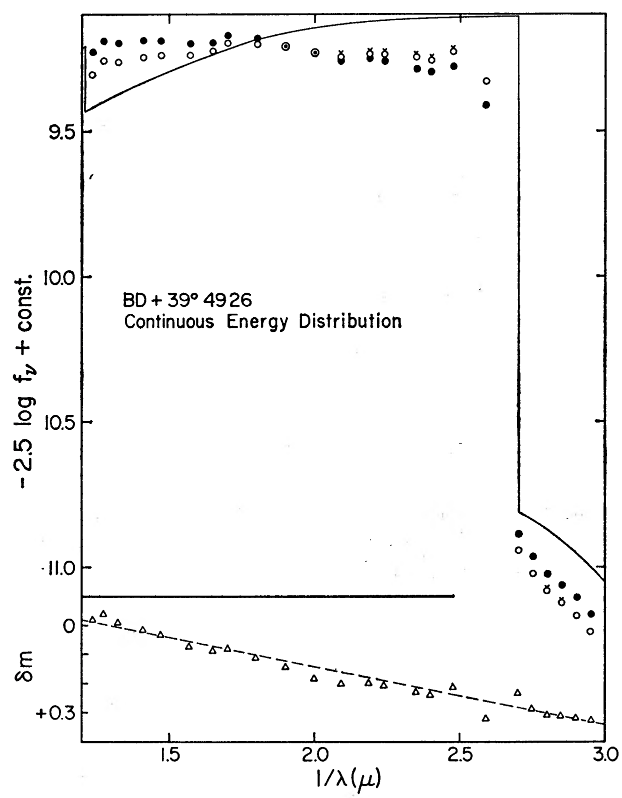

FIG. 8.—*Solid curve*, emergent flux f_ν for model M3; *filled circles*, raw observations; *open circles*, corrected f_ν, on the scale of the blanketed Vega model. *Crosses*, small effects of lines in Vega. Lower part of the figure shows the discrepancy in magnitudes with arbitrary zero, δm_ν, as a function of λ^{-1}. The linear behavior is consistent with interstellar reddening.

The bolometric correction, calculated relative to the horizontal-branch A star HD 161817 (Kodaira 1964), is $M_{\rm bol} - M_v = +0.06$ mag. The unreddened color of the M3 model is $B - V = 0.03$ mag, without correction for absorption lines.

The final model predicts Balmer-line profiles as shown in Figure 9. The observed profiles on the Pc and Pd plates are shown separately for Hβ; for Hα, only Pd plates exist. The Griem (1967) and Pfennig (1966) broadening theories are shown separately; they give significant differences only for Hα. The lower resolution of the Pd plates and the use of red-sensitive emulsions degrade the Hα profile. The Hβ profile fits the data from Pc plates. If we allow for the effect of lower resolution indicated by Hβ, as observed at 27 Å mm^{-1}, the Hα profile fits somewhat better with the theoretical profile of Pfennig. The very low density of the plasma makes a more detailed comparison of the Stark-effect theories unwise.

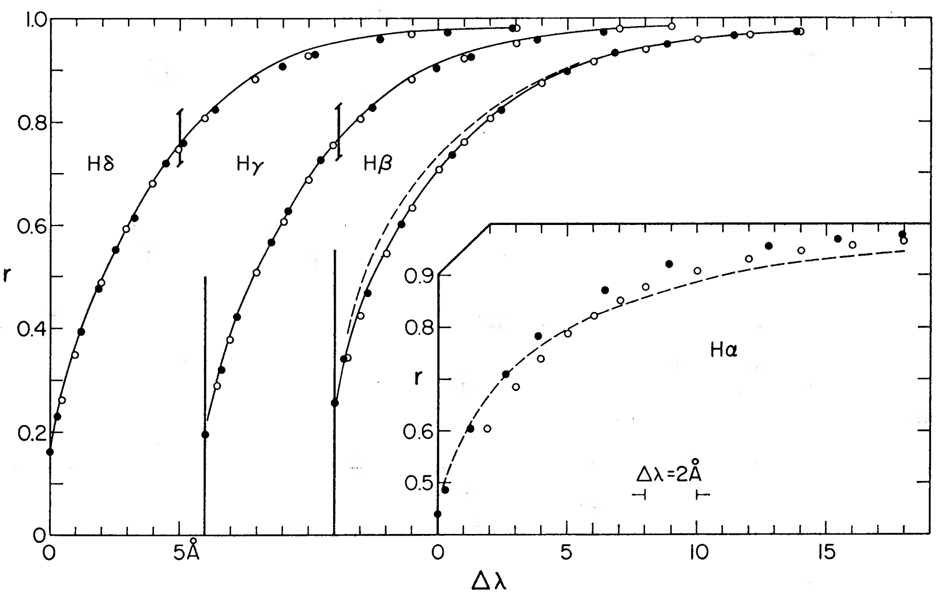

FIG. 9.—Observed Balmer lines (*solid lines*, Pc plates; *dashed lines*, Pd plates) and the line broadening calculated for M3, compared with the Griem theory (*open circles*) and Pfennig (*filled circles*). Vertical bars show effects of change from solution M1 to M2.

VII. CHEMICAL ABUNDANCES

Model M3 permits the prediction of line profiles and equivalent widths by standard machine routines. From each line strength W_λ, an abundance log ϵ is derived in Table 9, under the assumption of local thermodynamic equilibrium in ionization and excitation. We take log ϵ(H) = 12.00; the effect of helium will be discussed below. The gf-value used is listed with its source; the bibliography for gf-values is given in Table 11. When lines in a multiplet are blended, intrinsically or because of limited resolution, the transitions are bracketed, and the total W_λ is given for the blend. Blends with other elements are given in the last column. In several cases, blended lines were the only possible source for the abundance of a rare element or one with few observable lines. We therefore computed the blended line profile and subtracted that portion of the strength which originated in the blending component (for which the abundance was known from other lines). For several strong lines we needed the radiation-damping constants to determine log a and predict the profile. These are tabulated in the last column of Table 9 as γ, in units of 10^8 sec^{-1}. For other lines the classical damping constant was used. Assumption of constant microturbulence does not seem to lead to any contradiction, which would appear

TABLE 9

DATA FOR ABUNDANCE DETERMINATION

Transition		RMT	λ	χ_{rs} ev	log gf	f-source	W_λ	log ε	Remarks
C I ⟨log ε⟩ = 8.26									
$3s^1P^o$	$4p^1S$	(13)	4932.05	7.65	-1.78	NBS	69	8.34	
	^1P	(11)	5380.34	7.65	-1.68	NBS	67	8.21	
	^1D	(12)	5052.17	7.65	-1.49	NBS	98	8.28	
$3s^1P^o$	$5p^1S$	(17)	4228.33	7.65	-2.21	G	28	8.30	
	^1P	(14)	4371.37	7.65	-2.08	NBS	36	8.28	
	^1D	(16)	4269.02	7.65	-2.36	NBS	28	8.45	
$3s^3P^o$	$4p^3P$	(6)	4770.03	7.46	-2.25	G	24	8.11	
		(6)	4771.75	7.46	-1.70	NBS	60	8.03	
		(6)	4775.91	7.46	-2.20	NBS	40	8.31	
		(6)	4766.68	7.46	-2.40	NBS	24	8.25	
		(6)	4762.31	7.46	-2.28	NBS	}69	8.28	
		(6)	4762.54	7.46	-2.20	NBS			
O I ⟨log ε⟩ = 8.82									
3^5S^o	4^5P	(3)	3947.30	9.11	-2.05	G			
		(3)	3947.49	9.11	-2.20	G	}68	8.52	
		(3)	3947.59	9.11	-2.43	G			
3^3S^o	4^3P	(5)	4368.30	9.48	-1.65	G	58	8.82	
3^5P	5^5S^o	(9)	6453.64	10.69	-1.33	G			
		(9)	6454.48	10.69	-1.11	G	}60	8.60	FeII(74) blend
		(9)	6456.01	10.69	-0.97	G			
3^5P	4^5D^o	(10)	6155.99	10.69	-0.68	G			
		(10)	6156.78	10.69	-0.46	G	}264	8.95	
		(10)	6158.19	10.69	-0.31	G			
3^5P	6^5S^o	(11)	5435.16	10.69	-1.81	G			
		(11)	5435.76	10.69	-1.59	G	}97	9.32	
		(11)	5436.83	10.69	-1.44	G			
3^5P	5^5D^o	(12)	5328.98	10.69	-1.25	G			
		(12)	5329.59	10.69	-1.03	G	}148	8.99	
		(12)	5330.66	10.69	-0.88	G			
3^3P	6^3S^o	(22)	6046.26	10.94	-1.80	G			
		(22)	6046.46	10.94	-1.58	G	}38	8.61*	SI(10) blend
		(22)	6046.46	10.94	-2.28	G			
*If SI blend is ignored, log ε = 9.33									
Na I ⟨log ε⟩ = 3.80									
3^2S	3^2P^o	(1)	5889.95	0.00	+0.13	BL	30::	3.81	} blend with IS
		(1)	5895.92	0.00	-0.18	BL	15::	3.80	
Mg I ⟨log ε⟩ = 5.72									
3^3P^o	4^3S	(2)	5172.68	2.70	-0.40	T	124	5.69	γ = 1.0
		(2)	5183.60	2.70	-0.17	T	150	5.65	γ = 1.0
3^3P^o	3^3D	(3)	3838.29	2.70	}+0.51	T	213	5.76	γ = 2.6
		(3)	3838.29	2.70					
		(3)	3829.35	2.70	-0.19	T	92	5.35	γ = 2.6
		(3)	3832.30	2.70	}+0.29	T	208	5.90	γ = 2.6
		(3)	3832.30	2.70					
3^1P^o	6^1D	(14)	4351.89	4.33	}-1.00	A	88	6.26	γ = 2.6 FeII(27)blend Weight 1/2
			4351.90	4.33					
Mg II ⟨log ε⟩ = 5.65									
3^2D	4^2F^o	(4)	4481.13	8.83	+0.58	BL	}179	5.65	γ = 7.2
		(4)	4481.33	8.83	+0.75	BL			
Al I ⟨log ε⟩ = 3.23									
3^2P^o	4^2S	(1)	3961.52	0.01	-0.28	BL	17:	3.35	
		(1)	3944.01	0.00	-0.58	BL	4::	3.00	Weight 1/2

TABLE 9 (CONT'D)

Transition		RMT	λ	χ_{rs} ev	log gf	f-source	W_λ	log ε	Remarks
Si II ⟨log ε⟩ = 6.02									
3^2D	4^2P^o	(1)	3856.02	6.83	-0.74	H	70	5.79	
		(1)	3862.59	6.83	-0.97	H	40	5.67	
		(1)	3853.66	6.83	-1.69	H	26	6.15	
4^2S	4^2P^o	(2)	6347.09	8.09	+0.25	H	74	5.96	
		(2)	6371.36	8.09	-0.05	H	35	5.80	
3^2D	4^2F^o	(3)	4130.88	9.80	+0.40	H	32	6.13	
		(3)	4128.05	9.79	+0.22	H	25	6.16	
4^2P^o	4^2D	(5)	5056.02	10.03	+0.31	H	56::	6.86	Weight 1/2
		(5)	5056.35	10.03	-0.74	H			
		(5)	5041.06	10.03	+0.05	H	36::	6.92	
Ca II ⟨log ε⟩ = 3.24									
4^2S	4^2P^o	(1)	3933.66	0.00	+0.17	TB	435	3.24	blend with IS γ = 1.9
Sc II ⟨log ε⟩ = 0.35									
a^1D	z^1D^o	(7)	4246.83	0.31	+0.15	GR	23	0.20	
a^3F	z^3F^o	(14)	4415.56	0.59	-0.44	GR	13	0.45	FeI(41) blend
		(14)	4374.46	0.62	-0.06	GR	15	→	YII(13) blend
a^3F	z^3D^o	(15)	4314.08	0.62	+0.14	BD	22	0.40	FeII(32) blend
		(15)	4320.75	0.60	+0.20	GR	18:	0.26	
		(15)	4325.01	0.59	-0.20	GR	11:	0.43	
Ti II ⟨log ε⟩ = 1.82									
a^2F	z^2F^o	(13)	3759.29	0.60	+0.15	TA*	47	1.21	
		(13)	3761.32	0.57	-0.01	TA*	82	1.69	
a^2D	z^2F^o	(19)	4395.03	1.08	-0.30	TA	30	1.73	
		(19)	4443.80	1.08	-0.64	TA	20	1.88	
a^2D	z^2D^o	(20)	4294.10	1.08	-1.94	TA	14:	→	FeI(41) blend
a^2G	z^2F^o	(31)	4468.49	1.13	-0.52	TA	12	1.56	
		(31)	4501.27	1.11	-0.79	TA	15	1.92	
a^2G	z^2G^o	(34)	3900.55	1.13	-0.08	TA	37	1.75	
		(34)	3913.46	1.11	-0.20	TA	42	1.88	
a^4P	z^2D^o	(40)	4417.72	1.16	-1.15	TA	15:	2.32	Weight 1/2
a^4P	z^4D^o	(41)	4300.05	1.18	-0.40	TA*	24	1.81	
		(41)	4290.22	1.16	-0.68	TA*	18	1.95	
		(41)	4307.90	1.16	-1.00	TA	12	→	FeI(42) blend
a^2D	z^2D	(50)	4533.97	1.23	-0.59	TA*	34	2.20	
		(50)	4563.76	1.22	-0.84	TA	24:	2.26	Weight 1/2
a^2H	z^2G^o	(82)	4571.97	1.56	-0.24	TA	18	1.79	
Cr II ⟨log ε⟩ = 3.06									
a^4F	z^4F^o	(30)	4824.13	3.85	-0.79	GR	22::	3.34	Weight 1/2
		(30)	4848.24	3.85	-1.00	GR	21:	3.53	
		(30)	4876.41	3.84	-1.07	GR	19::	3.54	Weight 1/2
b^4F	z^4D^o	(44)	4558.66	4.06	+0.12	CB	26	2.69	
		(44)	4588.22	4.05	-0.07	GR	18	2.69	
		(44)	4618.83	4.06	-0.38	GR	19	3.02	
		(44)	4634.11	4.05	-0.49	GR	15:	3.01	
Fe I ⟨log ε⟩ = 4.32									
a^5D	z^5D^o	(4)	3859.91	0.00	-0.72	K	24	4.21	
a^5F	y^5D^o	(20)	3820.43	0.86	+0.22	K	40:	4.21	
		(20)	3825.88	0.91	+0.08	K	49:	4.51	
a^5F	y^5F^o	(21)	3758.24	0.95	+0.18	K	39::	4.32	Weight 1/2
a^3F	z^5G^o	(41)	4383.55	1.48	+0.50	K	25	4.13	
		(41)	4404.75	1.55	+0.21	K	17:	4.28	
		(41)	4415.13	1.60	-0.27	K	13	→	ScII(14) blend
		(41)	4294.13	1.48	-0.70	K	14:	5.02	TiII(20) blend

TABLE 9. (CONT'D)

Transition		RMT	λ	χ_{rs} ev	log gf	f-source	W_λ	log ε	Remarks
Fe I ⟨log ε⟩ = 4.32 (Cont'd)									
a^3F	z^3G^o	(42)	4271.76	1.48	+0.12	K	23	4.47	
		(42)	4307.91	1.55	+0.25	K	12:	3.70	TiII(41) blend
		(42)	4325.77	1.60	+0.31	K	24	4.40	
		(42)	4202.03	1.48	-0.37	K	10::	4.59	Weight 1/2
a^3F	y^3F^o	(43)	4045.82	1.48	+0.51	K	25	4.15	
		(43)	4063.60	1.55	+0.36	K	16	4.14	(CI blend)
		(43)	4071.74	1.60	+0.31	K	18	4.28	
z^7D	e^7D	(152)	4235.94	2.41	+0.40	C	16::	4.75	Weight 1/2
Fe II ⟨log ε⟩ = 4.33									
a^2P	z^4D^o	(14)	3783.35	2.27	-2.48	GRR	52::	5.05	Weight 1/2
b^4P	z^4D^o	(27)	4233.17	2.57	-1.12	GRR	108	4.36	
		(27)	4351.76	2.69	-1.20	GRR	88	→	MgI(14) blend
		(27)	4416.82	2.77	-1.78	GRR	21	4.21	
		(27)	4173.45	2.57	-1.77	GRR	28	4.20	
		(27)	4303.17	2.69	-1.72	GRR	35	4.34	
		(27)	4385.38	2.77	-1.70	GRR	18:	4.06	
b^4P	z^4F^o	(28)	4178.86	2.57	-1.46	GRR	35	4.00	
		(28)	4296.57	2.69	-2.17	GRR	18	4.47	
		(28)	4258.16	2.69	-2.55	GRR	15::	4.77	
a^4H	z^4F^o	(32)	4313.60	2.66	-3.20	GRR	22	→	ScII(15) blend
b^4F	z^4F^o	(37)	4629.34	2.79	-1.59	GRR	37	4.30	
		(37)	4555.89	2.82	-1.50	GRR	34	4.19	
		(37)	4515.34	2.83	-1.66	GRR	27	4.24	
		(37)	4491.40	2.84	-1.97	GRR	9::	4.06	
		(37)	4520.23	2.79	-1.73	GRR	25	4.24	
		(37)	4489.19	2.82	-2.08	GRR	16	4.42	
b^4F	z^4D^o	(38)	4583.83	2.79	-1.10	GRR	78	4.24	
		(38)	4522.63	2.83	-1.34	GRR	48	4.22	
		(38)	4508.28	2.84	-1.56	GRR	45	4.43	
		(38)	4541.52	2.84	-2.16	GRR	28	4.77	
a^6S	z^6P^o	(42)	5169.03	2.88	-0.54	GRR	135	4.17	
		(42)	5018.43	2.88	-0.64	GRR	147	4.38	
		(42)	4923.92	2.88	-0.75	GRR	108	4.18	
b^4D	z^4P^o	(74)	6456.38	3.89	-1.26	GRR	60	→	OI(9) blend
c^2F	x^2G^o	(173)	3935.94	5.54	-0.64	GRR	25::	5.19	Weight 1/2
Sr II ⟨log ε⟩ =-0.82									
5^2S	5^2P^o	(1)	4077.71	0.00	+0.16	GR	11	-0.88	
		(1)	4215.52	0.00	-0.14	GR	9::	-0.69	Weight 1/2
Y II ⟨log ε⟩ =-0.71									
a^1D	z^1D^o	(13)	4374.94	0.41	+0.24	HU	15	-0.80	ScII(14) blend
a^1D	z^3F^o	(14)	4177.54	0.41	-0.24	CB	9:	-0.54	

TABLE 10

DATA FOR ABUNDANCE DETERMINATION

(Uncertain lines)

Transition		RMT	λ	χ_{rs}	log gf	f-source	W_λ	log ε	Remarks
He I ⟨log ε⟩ = 12.15									
z^3P^o	4^3D	(14)	4471.48	20.87	-0.01	TSDJ	23::	12.02	γ = 2.84
2^3P^o	5^3D	(18)	4026.19	20.87	-0.43	TSDJ	}21:	11.82	γ = 2.44
		(18)	4026.36	20.87	-1.33	TSDJ			
2^3P^o	6^3D	(22)	3819.61	20.87	-0.67	TSDJ	}41::	12.61	γ = 2.30
			3819.76	20.87	-1.57	TSDJ			
N I ⟨log ε⟩ = 8.37									
$3s^4P$	$4p^4S^o$	(6)	4151.46	10.29	-1.87	NBS	6::	8.05	
$3s^2P$	$3p'^2D^o$	(10)	4109.98	10.64	-1.21	NBS	30::	8.41	
$3p^2S^o$	$4d^2P$	(16)	6008.48	11.55	-1.21	G	≲10	7.94	
$3p^4P^o$	$5s^4P$	(20)	6644.96	11.71	-0.91	NBS	25::	9.08	
Ne I log ε <9.76									
$3s1^o$	3p2	(1)	6402.25	16.55	+0.27	NBS	< 8::	<9.76	
S I ⟨log ε⟩ = 7.34									
4^5S^o	5^5P	(2)	4694.13	6.50	-1.91	M	11::	7.12	
		(2)	4695.45	6.50	-2.06	M	10::	7.23	
		(2)	4696.25	6.50	-2.28	M	4::	7.04	
4^5P	5^5D	(8)	6757.16	7.84	-0.36	GMA	71::	7.54	
		(8)	6748.79	7.84	-0.51	KD	43::	7.40	
		(8)	6743.58	7.84	-0.73	KD	44::	7.63	
4^5P	6^5D^o	(10)	6052.66	7.84	-0.67	GMA	30::	7.36	
		(10)	6046.04	7.83	-0.82	KD	38	7.36	OI(22) blend
4^5P	7^5D^o	(11)	5706.11	7.84	-----	---	50	----	

as a dependence of log ϵ on W_λ. The $\langle \log \epsilon \rangle$ for each element from the given stage of ionization, including weights by line quality, is given at the top of each group of lines used. The observed ionization level is correct for Fe and Mg, as would be expected from Figure 7, where atmospheric parameters determined by different methods agree moderately well.

In Table 10 we present information based on weak and uncertain lines of critically important elements, He, N, Ne, and S. There seems little doubt that the helium lines are present, in spite of the low effective temperature. Since no emission lines were seen, chromospheric enhancement of He I absorption seems unlikely. Keenan and Greenstein (1963) reported He I in R CrB, which is an even cooler carbon star. Because of the high

TABLE 11

SOURCES OF *f*-VALUES

NBS	Wiese, W. L., Smith, M. W., and Glennon, B. M. 1966, *Atomic Transition Probabilities*, NSRDS-NBS4, Vol. **1**.
G	Griem, H. R. 1964, *Plasma Spectroscopy* (New York: McGraw-Hill Book Co.), and 1964, *NRL Rept.*, No. 6085.
TSDJ	Trefftz, E., Schlüter, A., Dettmar, K. H., and Jürgens, K. 1957, *Zs. f. Ap.*, **44**, 1.
GMA	Goldberg, L., Müller, E. A., and Aller, L. H. 1960, *Ap. J. Suppl.*, **5**, 1.
M	Miller, M. H. 1968, University of Maryland Tech. Note BN-50.
BL	Biermann, L., and Lübeck, K. 1948, *Zs. f. Ap.*, **25**, 325.
T	Trefftz, E. 1950, *Zs. f. Ap.*, **28**, 67.
A	Allen, C. W. 1957, *M.N.R.A.S.*, **117**, 622.
H	Hey, P. 1959, *Zs. f. Phys.*, **157**, 79.
TB	Trefftz, E., and Biermann, L. 1952, *Zs. f. Ap.*, **30**, 275.
TA	Tatum, J. B. 1961, *Com. Univ. London Obs.*, No. 44. (See Groth *et al.* [1961].)
GR	Groth, H. G. 1961, *Zs. f. Ap.*, **51**, 231.
GRR	Groth, H. G. 1961, *Zs. f. Ap.*, **51**, 231; Roder, O. 1962, *Zs. f. Ap.*, **55**, 38; Baschek, B., Kegel, W. H., and Traving, G. 1963, *Zs. f. Ap.*, **56**, 282: log *f* (GRR) = log *f* (GR) + 0.96.
CB	Corliss, C. H., and Bozman, W. R. 1962, *N.B.S. Monog.*, No. 53.
K	King, R. B., and King, A. S. 1938, *Ap. J.*, **87**, 24; Bell, G. D., Davis, M. H., King, R. B., and Routly, P. M. 1958, *Ap. J.*, **127**, 775: log *f*(K) = log *f* (King, King) −3.27.
C	Carter, W. W. 1949, *Phys. Rev.*, **76**, 962; normalized in the same way as K.
HU	Hunger, K. 1955, *Zs. f. Ap.*, **36**, 42.
BD	Calculated by K. Kodaira in Coulomb approximation after Bates, D. R., and Damgaard, A. 1949, *Phil. Trans. Roy. Soc. London, A*, **242**, 101.

excitation potential, the abundance is very sensitive to θ_e; helium is neutral, so that the logarithm of the population of the excited level varies as 20.87 θ. If there is no error in the distribution of the temperature in the model, and if we wish arbitrarily to reduce the helium abundance to normal values, which require a change $\Delta \log \epsilon = -1.2$, we must decrease θ_e by about 0.06. We then are completely outside the temperature domain covered by Figure 7. The N I lines are also very weak, and give a large scatter in individual determinations of log ϵ; the value for Ne I is only an upper limit; lines of S I ,while weak, seem to be present and give accordant results. We may assume that blending with unrecognized other elements makes log ϵ for all elements in Table 10 upper limits, although we believe that this overstates the likely errors, since all lines are so weak.

Sources of *f*-values are listed in Table 11. No good oscillator strengths were available for most of the weak C I lines, since even their multiplet designations were only recently published. Since the C I abundance is fairly well established by well-identified lines, we can derive stellar *gf*-values for all C I lines present in +39°4926 by using the well-determined $\langle \log \epsilon \rangle = 8.26$ for C I and then reading from the observed line strength the hitherto unknown gf-value. These additional C I lines are given in Table 12. Their W_λ are often poor, and since weak blends may be present, the gf-values should be upper limits. Their scale is based on good C I lines in Table 9 which have recent N.B.S. and Griem (G) computations of gf. When we compare the stellar gf-values with those computed in the Coulomb approximation by Griem (G) and by Kodaira (BD), there is a large systematic difference, about a factor of 10, as shown by Δ in the last column of Table 12. Either many of the C I lines are blended or the Coulomb-approximation results are poor for the mixed coupling of the high levels of C I. A few unresolved triplets arise from high levels of the O I quintet system; stellar f-values deduced in Table 12, $\log gf = -1.30$ and -1.99, seem reasonable since $3^5\ P$–5^5D^o has a summed $\log gf = -0.57$. The series of C I and O I lines in +39°4926 is observed to higher numbers than in the older laboratory sources.

TABLE 12

STELLAR OSCILLATOR STRENGTHS FOR C I AND O I AS DERIVED FROM +39°4926

Transition	RMT	λ	χ_{rs}	W_λ	$\log gf(*)$	$\log gf$	Δ
C I:							
$3s^1P^o\ 6p^1S$...........	...	3942.22	7.65	15::	−2.45	...	...
^1P...........	...	4009.93	7.65	10::	−2.64	...	...
$3s^3P^o\ 5p^3P$...........	...	4029.41	7.46	12::	−2.70	−3.37BD	0.67
	(7)	4064.27	7.46	14::	−2.63	−3.37G	0.74
	(7)	4065.25	7.46	16::	−2.54	−3.64G	1.10
$3p^3D\ 5d^3D$...........	...	6006.03	8.61	30	−1.42	−3.28BD	1.86
	...	6013.22	8.61				
$3p^3D\ 6s^3P^o$..........	...	6013.22	8.61	124	−0.74	−1.10BD	0.36
	...	6014.85	8.61				
	...	6007.18	8.61	45	−1.17	−2.14BD	0.93
	...	6010.68	8.61	54	−1.11	−2.01BD	0.90
	...	6001.13	8.61	43	−1.24	−2.24BD	1.00
$2p'^3D^o\ 5p^3P$..........	...	4738.21	7.94	28::	−2.29	...	...
	...	4738.47	7.94				
	...	4734.26	7.94	16::	−2.23	...	...
$2p'^3D^o\ 5fF$..........	...	4477.47	7.94	9::	−2.49	...	...
	...	4478.32	7.94				
	...	4478.56	7.94	25:	−2.04	...	...
	...	4478.83	7.94				
$2p'^3D^o\ 5fG$..........	...	4466.68	7.94	11	−2.40	...	...
$2p'^3D^o\ 6fF$..........	...	4223.36	7.94				
	...	4223.16	7.94	21	−2.11	...	...
	...	4223.16	7.94				
$2p'^3D^o\ 7fG$..........	...	4072.64	7.94	7::	−2.59	...	...
O I:							
$3^5P\ 6^5D^o$...........	(14)	4967.40	10.69				
	(14)	4967.86	10.69	28::	−1.30	...	...
	(14)	4968.76	10.69				
$3^5P\ 7^5D^o$...........	(16)	4772.54	10.69				
	(16)	4772.89	10.69	19	−1.99	...	...
	(16)	4773.76	10.69				

VIII. RÉSUMÉ OF FINAL ABUNDANCES AND DISCUSSION

The mean log ϵ are collected in Table 13 for all elements which we can study in +39°4926. To compare with a "normal" stellar value, the differences are tabulated in the fifth column, and the number of lines, n, is given in the last column. The "normal" abundances are based on the Sun (Goldberg, Müller, and Aller 1960; Zwaan 1962) and those for He and Ne on the early-type stars (Traving 1955, 1957, 1958; Aller, Elste, and Jugaku 1956; Aller and Jugaku 1959; Jugaku 1959; Scholz 1967). Values in parentheses are highly uncertain; in general, they should be viewed as upper limits, although lines of the element may be present. The boldface numbers have relatively high accuracy, i.e., errors of $\Delta \log \epsilon \lesssim 0.3$; other elements, except for those in parentheses, have errors near 0.5. The $\Delta \log \epsilon$ give a comparison of abundance with those in the Sun and Population I stars. The major results are an iron-group deficiency by a logarithmic factor of −2.5,

TABLE 13

CHEMICAL ABUNDANCES IN THE ATMOSPHERE OF +39°4926

Element (1)	Z (2)	log ε: Normal (3)	log ε: +39°4926 (4)	Δ log ε (5)	n (6)
H.......	1	12.00	12.00	...	...
He......	2	11.20	(12.15)	(+0.95)	3
C.......	6	8.72	**8.26**	**−0.46**	11
N.......	7	7.98	(8.37)	(+0.39)	4
O.......	8	8.96	**8.82**	**−0.14**	7
Ne......	10	(8.70)	(<9.76)	(<+1.06)	1
Na......	11	6.30	3.80	−2.50	2
Mg......	12	7.36	**5.69**	**−1.67**	7
Al......	13	6.20	3.23	−2.97	2
Si......	14	7.45	**6.02**	**−1.43**	9
S.......	16	7.30	(7.34)	(+0.04)	8
Ca......	20	6.15	3.24	−2.91	1
Sc......	21	2.82	**0.35**	**−2.47**	5
Ti......	22	4.68	**1.82**	**−2.86**	14
Cr......	24	5.36	**3.06**	**−2.30**	7
Fe......	26	6.47	**4.33**	**−2.14**	38
Sr......	38	2.60	−0.82	−3.42	2
Y.......	39	2.25	−0.71	−2.96	2

indications of a larger deficiency −3.2 of the heavier elements, and quite high, nearly normal abundances, $\Delta \log \epsilon$, averaging −0.1, for C, N, O, and possibly S. There is possibly also an excess of helium.

A red giant of the globular-cluster type showed a similar pattern of deficiencies for the heaviest elements (Wallerstein *et al.* 1963), but the abundance of oxygen could not be determined. Nearly solar values of the O abundance occur for slightly metal-poor stars like α Boo (Conti *et al.* 1967) and for the horizontal-branch A stars HD 161817 (Kodaira 1964, 1967), and are suggested for HD 86986 and HD 109995 (Kodaira, Greenstein, and Oke 1969). The abundance of C was found, however, to be low in the extremely metal-weak Population II, sdG star HD 140283 (Baschek 1959, 1962) and, with considerable uncertainty, also low in an sdK, HD 25329 (Pagel and Powell 1966). There are some discrepancies between the C and O abundances deduced from molecular bands in the G and K stars, as, for example, their low abundance in HD 2665 and HD 6755 (Koelbloed 1967), and differences between Pagel (1965), Pagel and Powell

(1966), and Baschek (1959, 1962). However, in +39°4926 the problems of molecular equilibria do not arise, and there is little doubt concerning the very large difference in $\Delta \log \epsilon$ between the iron group and C and O.

If there are no systematic errors, such as would be caused by errors in the effective temperature or in the model, the pattern of abundance deficiencies is a very extreme one. The star has nearly the largest iron-group deficiency, and the most extreme variation with Z. In addition, with considerable certainty, C and O have high abundances. Different types of stars are known with all these peculiarities; e.g., the G subdwarfs have nearly as great an iron-group deficiency, HD 122563 has a low ratio of Y, Ba to Fe, α Boo has a slight metal deficiency but normal O, and the CH stars have high C. The odd-even alternation in abundance deficiencies (Na and Al as compared with Mg and Si) is a new phenomenon.

The low temperature makes the presence of He I difficult to understand; furthermore, the use of highly excited lines of C I, N I, O I, Mg II, and Si II (6–9 eV) might conceivably render the abundances temperature-sensitive. The complicated balance between excitation and ionization, however, makes it necessary to examine this suggestion in detail. Since we had a reasonably good network of model atmospheres, we proceeded as follows. We chose computed models with values for θ_{eff} of 0.65, 0.685, and 0.70 at log $g = 1.0$, and another at $\theta_{\text{eff}} = 0.67$ with log $g = 1.2$. The models should be relatively accurate, since line blanketing by the metals must be negligible. The resonance continua of He, C, and O cannot have any effect, since they lie in the far-ultraviolet; it is hard to see why unusual continua like C^- and O^- should rival H and H^- and scattering. Neutral metals are too highly ionized. Consequently, a calculation was made of the effective population of the typical levels (means of those used in Table 10), for He I, C I, N I, O I, Na I, Mg II, Al I, Si II, Fe I, and Fe II. The value of $\log \eta_0$ was evaluated at $\tau_0 = 0.1$ for each atom or ion, with the Saha and Boltzmann factors as evaluated in LTE. The first result was that the dependence on surface gravity was negligible within the range of the error circle given by the Hγ and the BJ (Fig. 7). The temperature dependence, of course, varied greatly between low levels of neutral atoms (e.g., Na I) and highly excited levels of ions (e.g., Mg II). However, for the important, abundant elements C I, N I, and O I, the temperature dependence proved to be very small. Changes in ionization and excitation are roughly balanced by the opacity. From $\theta = 0.65$ to $\theta \leq 0.70$, $\log \eta_0$ for C I increases by 0.40, while $\log \eta_0$ for N I and O I has a flat maximum with a range of about 0.15; $\log \eta_0$ for Mg II is flat, and $\log \eta_0$ for Si II has a flat minimum with a range of 0.10. (This range of θ_{eff} covers most of Fig. 7.) However, as can be expected, $\Delta \log \eta_0/\Delta\theta$ is very large (about -24) for He I, and is $+15$ for Na I and Al I.

We explore solutions at higher T_{eff} than our final model, M3, since these reduce the He overabundance. If we do so, however, we do not change C, N, O, Mg, or Si, but increase only Na, Al, Y, Sr, and the abundance of Fe deduced from Fe I. Reduction of θ_{eff} by 0.02 (to M1) puts the solution just outside the range of plausibility for Hγ and BJ. It reduces the He overabundance, $\Delta \log \epsilon$, by only -0.5, and raises $\Delta \log \epsilon$ for Na and Al by $+0.3$. Referring to Figure 11, we see that the effect of raising Na and Al is to reduce the odd-even alternation by about one-third. The effect on Y and Sr is to increase their abundance relative to Fe by about 0.20, reducing the s-process deficiencies slightly. If we wish to obtain nearly the same abundance from Fe I and Fe II, we should also increase log g by about 0.3. This will not affect most $\Delta \log \epsilon$, since the decrease in ionization is balanced by the increase in opacity.

We may, finally, consider the effect of errors in the gf-scales for Fe I and Fe II. Based in part on [Fe II], some controversy now exists on the solar photospheric abundance of Fe; a discrepancy, in hot stars, between results from Fe III and Fe II is also related to this question. If $\log gf$ for both Fe I and Fe II scales are in error by the same amount, our ionization equilibrium is unaffected—$\log \epsilon$ is changed, but $\Delta \log \epsilon$ with respect to the Sun is not affected. But if an error of, say, a factor of 2 exists in $\log gf(\text{Fe II}) - \log gf(\text{Fe I})$, the line representing the ionization equilibrium in Figure 7 could be raised or lowered by 0.3 in log P_e. The intersection with the Mg locus is very indeterminate. It moves to unacceptably large θ if lowered by 0.3; if raised, it suggests $\theta_{\text{eff}} \approx 0.62$. If this were true, the profile of Hγ and the BJ would be completely inexplicable. A more rational estimate of the effect of changing the gf-scales for Fe, consistent with the hydrogen spectrum, would be to adopt M1 ($\theta_{\text{eff}} = 0.65$, $\log g = 1.0$). This produces, again, only the small changes in $\Delta \log \epsilon$ previously described. Unless unknown physical effects are at work, the θ_{eff}, and therefore the abundances, seem reasonably certain.

IX. SPECULATIONS ON NUCLEOSYNTHESIS

Conti *et al.* (1967) had suggested that nucleosynthesis of C and O was very rapid in the early history of old disk stars in our Galaxy, e.g., in α Boo. While +39°4296 is not necessarily a very high-velocity star, it has the most extreme known metal deficiency of the Population II stars in the halo. It is unlikely that nuclear processes in the star reduced the surface metal abundances. We have two choices. (1) We may assume that its composition is that of the material out of which it was formed, i.e., that of the very oldest interstellar gas, contaminated by only traces of the iron-group elements and even less of heavier elements (Sr, Y) formed by neutron capture on the iron group. In that case, the (He), ***C***, (N), **O**, and (S) (where boldface and parentheses indicate good and doubtful results, respectively, as in Table 13) had essentially the same abundances as when the Sun was formed, say, 5×10^9 years later, or the recent Population I stars, 10×10^9 years later. (2) Or, we may assume that the star was initially nearly pure hydrogen and equally deficient in all elements, but that (He), ***C***, (N), ***O***, and (S) were synthesized and, because of instabilities, the helium flash, or mass loss, brought to the surface. The second hypothesis, if correct, also requires that the primeval metals of Population II were poor in neutron-processed materials (i.e., little *s*-process). However, there are many difficulties in understanding the long-term survival of a massive star with a core sufficiently hot to undergo carbon burning, without a collapse or explosion. Certainly, if S is so synthesized, we are far beyond the end of a plausible chain of α-particle captures in a star of moderate mass (e.g., about 1.5 $M_\odot$, if it is a Population II star). Thus if the S abundance is reliable, we require operation of other processes for it to be produced in solar abundance. If we confine ourselves to He, C, N, and O, which are more reliable, we can use the results of Cameron (in his unpublished *Yale Lecture Notes in Nuclear Astrophysics*), Deinzer and Salpeter (1964), and Cox and Salpeter (1964). Essentially, low-mass stars of pure He, after evolution, will exhaust He and produce ^{12}C and ^{16}O, with negligible amounts of Ne or heavier elements. Only for $M > 25\ M_\odot$ does any Mg form, and our Table 13 shows that $\Delta \log \epsilon$ is -1.67 for Mg and -1.43 for Si, i.e., low abundances, but still less extreme than are the iron-group deficiencies. The uncertainties in reaction rates are such that from 0 to 60 percent of the He can be converted into ^{12}C when ^{4}He is exhausted (see, e.g., Figs. 5–21 to 5–31 in Clayton 1968). Since we observe O/C ≈ 3.5, our results are in a plausible range of Cameron's parameter R_{12} (destruction of ^{12}C) and R_{16} (destruction of ^{16}O). Since R_{16} seems small (negligible heavy elements synthesized), the central temperature required is not higher than 1.5×10^8 ° K and density 10^3 g cm^{-3}, about that of a degenerate core of low mass (Cox and Salpeter 1964) or a nondegenerate core of moderate mass. A star with 15 $M_\odot$, after helium exhaustion, however, has much too high an O/C ratio. We must definitely exclude initial very high mass, in which both C and O are destroyed by production of ^{20}Ne or ^{24}Mg. The stability of sulfur is low; if the high ratio S/Si is correct, we may also exclude very high temperatures, such as produce photodisintegration of S to Si, before silicon burning occurs. We will omit further discussion of such very massive parent stars.

Some secondary reaction must be involved in producing the high N abundance; ^{14}N/^{12}C > 10 for hydrogen-burning in a hydrogen shell surrounding a ^{4}He and ^{12}C core, if there are sufficient protons to let the CNO cycle go to its equilibrium abundances.

Only limited proton exposure is possible for this star, a reasonable hypothesis if the high value of He/H is substantiated. If instabilities mix surface material with substantial amounts of core material, dominantly He, then the number of α-particles bound into the C, N, and O nuclei is only 2×10^{-4} that in the form of He; helium is far from exhausted. Under such circumstances, almost all models produce only ^{12}C. We can blame the peculiarities on a complex of instabilities and mass transfer such as was studied by Kippenhahn and Weigert (1967). Barnard 29, in M13 (Stoeckly and Greenstein 1968) is probably also a binary; however, its deficiencies of C, N, O, and heavier elements are all the same, $\log \epsilon = -1.30$.

X. COMPARISON WITH OTHER METAL-POOR STARS

In Figure 10 we attempt to show simultaneously the abundances in the Sun and in the very metal-poor stars. The odd-even alternation is preserved in all, and the deviations from solar abundance generally increase with increasing Z. There are complex

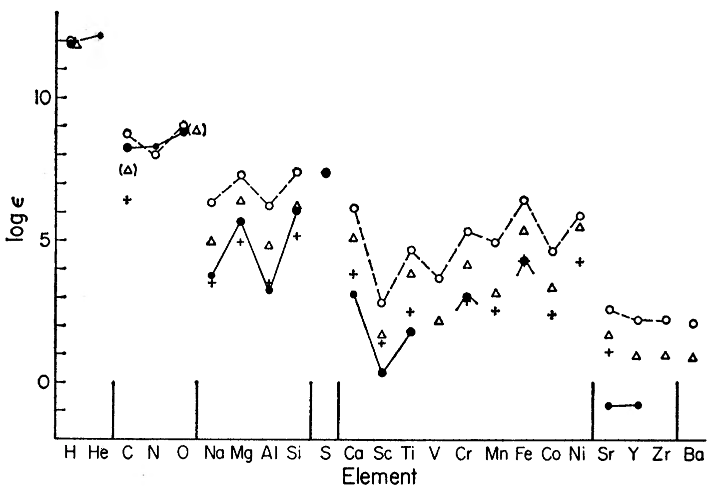

FIG. 10.—Elemental abundances, $\log \epsilon$, in the Sun (*open circles*) and in the metal-deficient stars +39°4926 (*filled circles*), HD 161817 (*triangles*), and HD 140283 (*crosses*). Vertical lines indicate gaps in the horizontal scale. The odd-even abundance alternation is displayed where possible, with a solid zigzag line for +39°4926 and a dashed line for the Sun.

effects in these deviations which may be real; those affecting C, N, and O are the most interesting. In Figure 11, a more detailed comparison of +39°4926 and the Sun is shown, where $\Delta \log \epsilon$ is plotted. The systematic decrease of relative abundance with Z is very striking. If we concentrate on the elements that might lie on an α-particle chain, or be involved in carbon burning, there is a very large decrease (by a factor of 1000) from C, O to Ca. Elements with odd Z lie below this general trend (except for N, which requires secondary processing). The elements at $Z = 38$–39 are more deficient, and since all lines are weak, no outstanding elemental excesses appear as heavy-element peaks. The very different halo stars, HD 161817, an A-type, horizontal-branch star, and HD 140283, an sdG, show deviations from the Sun in Figure 10 which run rather parallel. To simplify the diagram, we average $\Delta \log \epsilon$ for these two stars and plot them as crosses in Figure 11. The $\Delta \log \epsilon$'s for these halo stars are surprisingly constant, except for the primeval high abundance of O, which comes from HD 161817 only, and is uncertain, since HD 140283 does not show it. There is no odd-even alternation. The halo stars show in a much less clear manner the steep decrease from C, N, O to the iron group. But in +39°4926 the zigzag nature of the differences from the Sun is so marked that it is appealing to assume that synthesis of the elements occurred in a single event. An explosion of a massive single star may have contaminated the gas cloud out of which +39°4926 was formed, at a time when all elements but hydrogen and possibly helium were very rare. In that case, an α-particle chain terminating at small Z played an important part, since odd-Z elements like Na and Al are 16 times more deficient than Mg and Si. We have already shown that oxygen destruction was negligible.

XI. OTHER PROPERTIES OF THE STAR

The mass-luminosity ratio can be obtained through the relation

$$\log \frac{M/M_\odot}{L/L_\odot} = \log g/g_\odot + 4 \log \theta_e/\theta_{e\odot} = -3.72 . \tag{4}$$

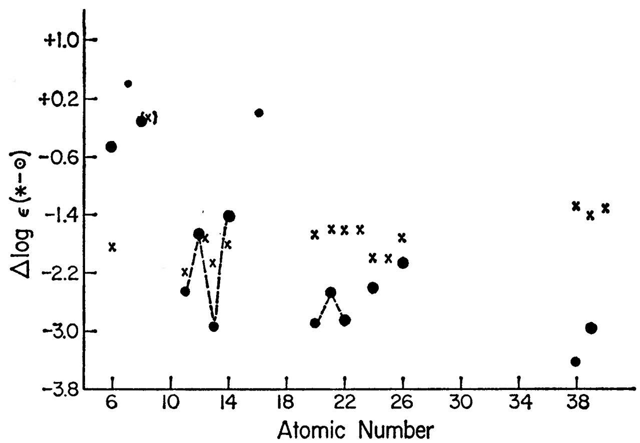

FIG. 11.—Abundance deficiencies, $\Delta \log \epsilon$, of +39°4926 compared with the Sun. Large filled circles have the highest weight; the smallest are poor determinations. Crosses show the $\Delta \log \epsilon$ between the averaged HD 161817 and HD 140283 and the Sun. Note rapid change with Z of abundances in BD +39°4926 (denoted by filled circles) and the rather constant $\Delta \log \epsilon$ in the halo stars. The odd-even effect is very pronounced at Z = 11–14.

With the bolometric magnitude of the Sun as +4.7, $\log g_\odot = 4.44$, $\theta_{e\odot} = 0.885$, we find

$$M_{\text{bol}} = -4.6 - 2.5 \log M/M_\odot . \tag{5}$$

With $M_v = M_{\text{bol}} - 0.06$, absorption of 0.3 mag, and $m_v = 9.1$, the distance r is given by

$$\log r = 3.67 + 0.5 \log M/M_\odot . \tag{6}$$

We will later assume that the observed star is the primary in a spectroscopic binary. The results are shown in Table 14 with parameters referred to star 1. The proper motion (*Smithsonian Star Catalog*, 1966) is extremely small, $\mu_\alpha = -0^{s}.001 \pm 0^{s}.001$, $\mu_\delta = +0''.007 \pm 0''.011$, so that the distance cannot be small. The percentage errors are so large that only rough values of space motions can be estimated, $V_\alpha = -46\, r_{\text{kpc}}$ from μ_α and $V_\delta = 33\, r_{\text{kpc}}$ from μ_δ. In the range of masses in Table 14, these range from about 60 to 400 km sec^{-1}. The range of distances from the galactic plane is 230–4200 pc. A mass of 1 $M_\odot$ seems a plausible maximum requiring space motions near 200 km sec^{-1}. However, the proper motion is so nearly zero that we can exclude only the largest or smallest masses. From the low radial velocity, it seems implausible that the space motion is large enough to produce the high Z-values required by the large mass solutions. A W-component velocity of 40 km sec^{-1}, which is the normal upper bound, occurs for 0.1 $M_\odot$. Kinematic as well as spectroscopic evidence precludes the star from being a runaway

Population I. The model with reasonable mass, 1 $M_\odot$, has $M_{\rm bol} = -4.6$ and is more luminous than globular-cluster W Virginis stars; except for the higher temperature, the 0.3 $M_\odot$, $M_{\rm bol} = -3.3$ model resembles the K giants found in globular clusters. Thus, a location in the region of rapid evolution and instability of type II stars is suggested.

A secondary effect, the possible very high abundance of helium, has been neglected in the above considerations. If log ϵ(He) = 12.2, as the weak, high-excitation lines indicated, then helium acts only as extra mass in the atmosphere. The same spectroscopic model would be derived with $\Delta \log R = -0.12$, $\Delta M_{\rm bol} = +0.65$, and $\Delta r/r = -0.35$. In Table 14 this is equivalent to an upward shift by about one-half the interval between the successive entries.

If the absorbing gas and dust are confined to a 0.15-kpc layer, the path length is about 0.5 kpc. The interstellar absorption of 0.3 mag gives about 0.6 mag per kpc (visual), a quite reasonable value. The statistical relations for interstellar line strengths given by Allen (1963) suggest r_0(kpc) = 3.1 W(K) and 2.0 W(D), where r_0 is the distance within the absorbing layer. The observed strengths in Table 6 give $r_0 = 0.32$ kpc from K and 1.5 kpc from D. Thus, the K-line strength seems reasonable, while the D-lines are anomalously strong. The cloud velocity, -20 km sec^{-1}, is just that expected from the solar motion and galactic rotation. As in other high-latitude stars, the Na I extends to greater heights than the Ca II, without excessively high velocities.

TABLE 14

RADIUS, BRIGHTNESS, DISTANCE, AS A FUNCTION OF THE ASSUMED MASS OF THE PRIMARY

log $M_1/M_\odot$	r (kpc)	log $R_1/R_\odot$	$M_{1,\rm bol}$	Mass Ratio μ	log $M_2/M_\odot$
−1.0	1.48	+1.12	−2.1	4.2	−0.38
−0.5	2.63	+1.37	−3.3	2.0	−0.20
−0.3	3.52	+1.47	−3.8	1.5	−0.12
0.0	4.7	+1.62	−4.6	1.0	+0.02
+0.5	8.3	+1.87	−5.8	0.60	+0.28
+1.0	14.8	+2.12	−7.1	0.37	+0.57

The observed stellar line widths of weak lines can be estimated as 0.4–0.5 Å, total width at half-intensity. After simple subtraction of the instrumental width (assumed to be more nearly damping than Gaussian) the residual width is found to be 16–22 km sec^{-1}. If we now treat this as a Gaussian profile, the $\Delta\lambda_{\rm D}$ = 10–14 km sec^{-1}. The microturbulence of 5 km sec^{-1} reduces this $\Delta\lambda_{\rm D}$ (subtracting by sums of squares) to the range 8–13 km sec^{-1}. If $\Delta\lambda_{\rm D} = v \sin i$, the projected macroturbulence plus rotational velocity is not more than 15 and probably less than 10 km sec^{-1}. The low rotation supports the hypothesis that the +39°4926 is more probably a highly evolved giant than a young supergiant (Kraft 1960). The observed macroturbulent and rotational line broadening in F supergiants of luminosity classes Ia and Ib (large-mass solution in Table 14) would be directly observable at 9 Å mm^{-1}. In fact, the metallic lines in +39°4926 appear quite sharp.

The binary-star hypothesis, if we assume a circular orbit, semiamplitude 15 km sec^{-1}, and period of 775 days (Fig. 1), leads to the mass function $f(m) = 1.035 \times 10^{-7} K_1^3 P = 0.27$. The mass ratio $\mu = M_1/M_2$ is unknown. The separation will be compared with the radius of the orbit of the visible star $a_1 \sin i = 1.5 \times 10^{13}$ cm. We have found no trace of the secondary in the line or continuous spectrum. Let $\sin i = 1$, and derive masses as a function of assumed μ, given in the last two columns of Table 14. Note that if the observed star is to be a massive Population I object, $\mu \approx 0.5$ gives a secondary of mass 2.4 $M_\odot$, i.e., a late B star, which would be on the main sequence only if the system is less than 5×10^8 years old. A mass ratio greater than unity accounts for the invisibility of the second star but leaves unexplained the rare evolutionary status of the primary. If $\mu = 1.5$, the secondary could be a quite undetectable white dwarf of 0.75 $M_\odot$, while the primary would have a mass of only 0.5 $M_\odot$. We could assume that the primary represents a normal, short-lived stage of Population II evolution. But the type of exchange of mass between evolving components of a binary suggested by Kippenhahn and Weigert (1967) might also be responsible for the unusual low masses for $\mu \geq 1.0$, and provides some reason for the unusual color and luminosity of the primary. Note that the best value of the radius $R = 2 \times 10^{12}$ cm is about 15 percent of the deduced $a_1 \sin i$. Thus, while the star is not now a contact binary, it could well have been one at an earlier stage of evolution, e.g., if it has reached its present temperature by evolution at constant luminosity from low to high temperatures. Furthermore, if we adopt a mass ratio of 0.37, i.e., the 10 $M_\odot$ solution in Table 14, the radius is 60 percent of $a_1 \sin i$ and the star should be a contact binary, with characteristic stream motions and emission lines, and these are not seen. In conclusion, if the velocity variation is that of a binary, the spectroscopic surface gravity gives the most probable solution as one with $M_1 < M_\odot$, i.e., a highly evolved Population II star, in agreement with the spectroscopic abundance anomalies.

The extremely long period is a significant objection to the pulsation hypothesis, e.g., if we assume that the star is related to W Virginis. If the $P\rho^{1/2}$ law is assumed to have the same pulsation constant as W Virginis, then +39°4926, which has about 20 times the period, has 2×10^{-3} the mean density. For equal mass, this requires a radius 10 times as large as that of W Virginis. But integration over the velocity curve gives a radius change of 1.6×10^{13} cm. Since the temperature and spectrum do not change during the cycle (e.g., constant f_ν), we should require the radius to be large compared with its change. If we adopt $R/\Delta R = 10$, then R is 1.6×10^{14} cm. At that radius the density of a star of 1 $M_\odot$ is far too low, about 10^{-10} g cm^{-3}; the surface gravity of 5×10^{-3} cm sec^{-2} is also incompatible with the spectroscopic observations. We have reexamined the original data obtained by Oke, on which a suspicion of light variability was based. Checking the data and photometric system for each night, together with the newly obtained data in this investigation, we find at most only slight variability.

This work was completed while one of us (J. L. G.) was at the Institute for Advanced Study.

REFERENCES

Allen, C. W. 1963, *Astrophysical Quantities* (2d ed.; London: Athlone Press).
Aller, L. H., Elste, G., and Jugaku, J. 1956, *Ap. J. Suppl.*, **3**, 1.
Aller, L. H., and Jugaku, J. 1959, *Ap. J. Suppl.*, **4**, 109.
Baschek, B. 1959, *Zs. f. Ap.*, **48**, 95.
———. 1962, *ibid.*, **56**, 207.
Baschek, B., Holweger, H., and Traving, G. 1966, *Abh. Hamburger Sternw.*, **8**, 26.
Baschek, B., and Oke, J. B. 1965, *Ap. J.*, **141**, 1404.
Bode, G. 1965, *Die Kontinueliche Absorption von Sternatmosphären*, Sonderdruck Kiel University.
Burbidge, E. M., Burbidge, G. R., Fowler, W. A., and Hoyle, F. 1957, *Rev. Mod. Phys.*, **29**, 547.
Clayton, D. D. 1968, *Principles of Stellar Evolution and Nucleosynthesis* (New York: McGraw-Hill Book Co.).
Conti, P., Greenstein, J. L., Spinrad, H., Wallerstein, G., and Vardya, M. S. 1967, *Ap. J.*, **148**, 105.
Cox, J. P., and Salpeter, E. E. 1964, *Ap. J.*, **140**, 485.
Deinzer, W., and Salpeter, E., E. 1964, *Ap. J.*, **140**, 499.
Gehlich, U. K. 1969, *Astr. and Ap.*, **3**, 169.
Goldberg, L., Müller, E. A., and Aller, L. H. 1960, *Ap. J. Suppl.*, **5**, 1.
Greenstein, J. L. 1968, *Ap. J.*, **152**, 431.
Griem, H. R. 1967, *Ap. J.*, **147**, 1092.
Hardorp, J., and Scholz, M. 1968, *Zs. f. Ap.*, **69**, 350.

Hayes, D. 1967, unpublished thesis, University of California at Los Angeles.
Heintze, J. R. W. 1968, *B.A.N.*, **20**, 1.
Johansson, L. 1966, *Ark. f. Fys.*, **31**, 201.
Jugaku, J. 1959, *Pub. Astr. Soc. Japan*, **11**, 161.
Keenan, P. C., and Greenstein, J. L. 1963, *The Line Spectrum of R Coronae Borealis* (Delaware, Ohio: Ohio State University and Mount Wilson and Palomar Observatories special reprint).
Kippenhahn, R., and Weigert, A. 1967, *Zs. f. Ap.*, **65**, 251.
Kodaira, K. 1964, *Zs. f. Ap.*, **59**, 139.
———. 1967, *Pub. Astr. Soc. Japan*, **19**, 550.
Kodaira, K., Greenstein, J. L., and Oke, J. B. 1969, *Ap. J.*, **155**, 525.
Koelbloed, D. 1967, *Ap. J.*, **149**, 299.
Kraft, R. P. 1960, *Stellar Atmospheres*, ed. J. L. Greenstein (Chicago: The University of Chicago Press), chap. 9.
Mihalas, D. 1965, *Ap. J. Suppl.*, **9**, 321.
———. 1966, *ibid.*, **13**, 1.
Oke, J. B. 1964, *Ap. J.*, **140**, 689.
———. 1965, *Ann. Rev. Astr. and Ap.*, **3**, 23.
Oke, J. B., Greenstein, J. L., and Gunn, J. 1966, *Stellar Evolution*, ed. R. F. Stein and A. G. W. Cameron (New York: Plenum Press), p. 399.
Pagel, B. E. J. 1965, *R.O.B.*, No. 104.
Pagel, B. E. J., and Powell, A.L.T. 1966, *R.O.B.*, No. 124.
Pfennig, H. 1966, *Zs. f. Naturforschung*, **21a**, 1648.
Sargent, W. L. W. 1965, *Observatory*, **85**, 116.
Scholz, M. 1967, *Zs. f. Ap.*, **65**, 243.
Smithsonian Astrophysical Obs. 1966, *Smithsonian Star Catalog* (Washington, D.C.: Smithsonian Institution).
Stoeckly, R., and Greenstein, J. L. 1968, *Ap. J.*, **154**, 1909.
Strom, S. E., Gingerich, O., and Strom, K. M. 1966, *Ap. J.*, **146**, 880.
Traving, G. 1955, *Zs. f. Ap.*, **36**, 1.
———. 1957, *ibid.*, **41**, 215.
———. 1958, *ibid.*, **44**, 142.
Wallerstein, G., Greenstein, J. L., Parker, R., Helfer, H. L., and Aller, L. H. 1963, *Ap. J.*, **137**, 280.
Wrubel, M. H. 1949, *Ap. J.*, **109**, 66.
Zwaan, C. 1962, *B.A.N.*, **16**, 255.